Available online at www.sciencedirect.com
SCIENCE DIRECT®
Sedimentary Geology 184 (2006) 77–109
Sedimentary Geology
www.elsevier.com/locate/sedgeo

The Cretaceous–Paleogene (K–P) boundary at Brazos, Texas: Sequence stratigraphy, depositional events and the Chicxulub impact

Peter Schulte [a,*], Robert Speijer [b], Hartmut Mai [c], Agnes Kontny [d]

[a] *Institut für Geologie und Mineralogie, Universität Erlangen-Nürnberg, Schloßgarten 5, D-91054 Erlangen, Germany*
[b] *Department of Geography and Geology, KU Leuven, Redingenstraat 16, B-3000 Leuven, Belgium*
[c] *Fachbereich 5 Geowissenschaften, Universität Bremen, Postfach 330440, D-28334 Bremen, Germany*
[d] *Geologisch-Paläontologisches Institut, Universität Heidelberg, Im Neuenheimer Feld 234, D-69120 Heidelberg, Germany*

Received 25 February 2005; received in revised form 14 September 2005; accepted 22 September 2005

Abstract

Two cores from Brazos, Texas, spanning the Cretaceous–Paleogene (K–P) boundary, are investigated by a multidisciplinary approach aiming at unraveling environmental changes and sequence stratigraphic setting. In addition, the sedimentology of the K–P event deposit and its correlation with the K–P boundary is studied. Foraminifera and nannofossil stratigraphy indicates that both cores include a latest Maastrichtian (Zone CF1–CF2) and earliest Danian (P0, Pα and P1a) shale sequence with a sandy and Chicxulub ejecta-bearing event deposit at the K–P boundary; a hiatus of unknown duration may be present by the unconformable base of the event deposit. Planktic foraminifera as well as calcareous nannofossil abundance and diversity both decline abruptly above the event deposit (K–P mass extinction), whereas benthic foraminifera show a pronounced faunal change but no mass extinction.

Mineralogical and geochemical proxies suggest that–except for the sandwiched K–P event deposit–no facies change took place across the K–P boundary and no evidence for adverse an- or dysoxic sedimentary conditions following the Chicxulub impact was observed. Therefore, the interval bracketing the K–P event deposit is considered as highstand systems tract. Increased coarse detritus input and low planktic/benthic (P/B) foraminifera ratios during the earliest Paleocene (P0 and Pα) both suggest an increased coastal proximity or relative sea-level lowering, although the K–P mass extinction of planktic foraminifera might have influenced the P/B ratios as well. Consequently, the sandy shales of the early Paleocene are considered as late regressive highstand or as lowstand deposit. During P1a, shales assigned as transgressive systems tract overlie a pyrite- and glauconite-rich bioturbated transgressive surface or type-2-sequence boundary. The smectite-dominated clay assemblage, with minor illite, kaolinite and chlorite indicates semiarid–humid climates with no obvious shifts across the K–P boundary. The magnetic susceptibility signature during the Maastrichtian reveals a subtle cyclic (or rhythmic) pattern, whereas a high-amplitude cyclic pattern is present during the early Danian.

The K–P event deposit shows a succession of high-energetic debris flows and turbidites derived from multiple source areas, followed by a period of decreasing current energy. Deposition was likely triggered by multiple tsunami or tempestites followed by a prolonged period of reworking and settling. The Chicxulub ejecta at the base of the K–P event deposit consists of Mg-rich smectite- as well as Fe–Mg-rich chlorite–spherules. Their mineralogical composition points to target rocks of mafic to intermediate composition, presumably situated in the northwestern sector of the Chicxulub impact structure. Besides these silicic phases, the most prominent ejecta components are limestone clasts, accretionary carbonate clasts, and microspar, suggesting that the Texas area received ejecta also from shallow, carbonate-rich lithologies at the impact site on the Yucatán carbonate platform. The excellent

* Corresponding author. Tel.: +49 9131 85 29240; fax: +49 9131 85 29295.
E-mail addresses: schulte@geol.uni-erlangen.de (P. Schulte), robert.speijer@geo.kuleuven.ac.be (R. Speijer), hmai@uni-bremen.de (H. Mai), agnes.kontny@urz.uni-heidelberg.de (A. Kontny).

0037-0738/$ - see front matter
doi:10.1016/j.sedgeo.2005.09.021

correlation of Chicxulub ejecta at Brazos with ejecta found in the K–P boundary layer worldwide – along with the associated mass extinction – provides no evidence that Chicxulub predated the K–P boundary and allows for unequivocal positioning of the K–P boundary at the event deposit.

Keywords: K–P boundary; Texas; Brazos; Sequence stratigraphy; Sea-level; Chicxulub impact; Ejecta

1. Introduction

Establishing a causal link between the mass extinction and the impact event at the Cretaceous–Paleogene (K–P) boundary has continued to attract geoscientists since the discovery of the Chicxulub impact site in southern Mexico (e.g., Ryder et al., 1996; Koeberl and MacLeod, 2002). Despite compelling evidence for the relationship between this impact event and the mass extinction, it is argued that gradual biotic and environmental changes preceded the impact level, deteriorating the Late Cretaceous fauna and flora (e.g., Keller et al., 1998a). Among the additional mechanisms of global change prior to the K–P boundary are Deccan Trap volcanism, multiple impacts, sea-level fluctuations, and climate change (Keller and Stinnesbeck, 1996; Hallam and Wignall, 1999; Wignall, 2001).

The study of marine sediments from the northwestern Gulf of Mexico has played a central role in this discussion. Prominent K–P localities from along this region include Mimbral (NE Mexico), Braggs (Alabama), and Brazos River in Texas (Fig. 1; Smit et al., 1996). Specifically, the shales and marls exposed along the Brazos River in Texas provide an excellent opportunity for studying the K–P boundary since they bear an expanded record of environmental and ecological changes across the boundary (Hansen et al., 1987, 1993a,b; Keller, 1989a). In addition, the Brazos K–P sections include an event deposit that is frequently present in Gulf of Mexico K–P sections and reveals evidence for the sedimentary disturbances and ejecta associated with the Chicxulub impact event (Bourgeois et al., 1988; Yancey, 1996; Heymann et al., 1998). This event deposit has been interpreted as incised channel fill resulting from a latest Maastrichtian lowstand (Stin-

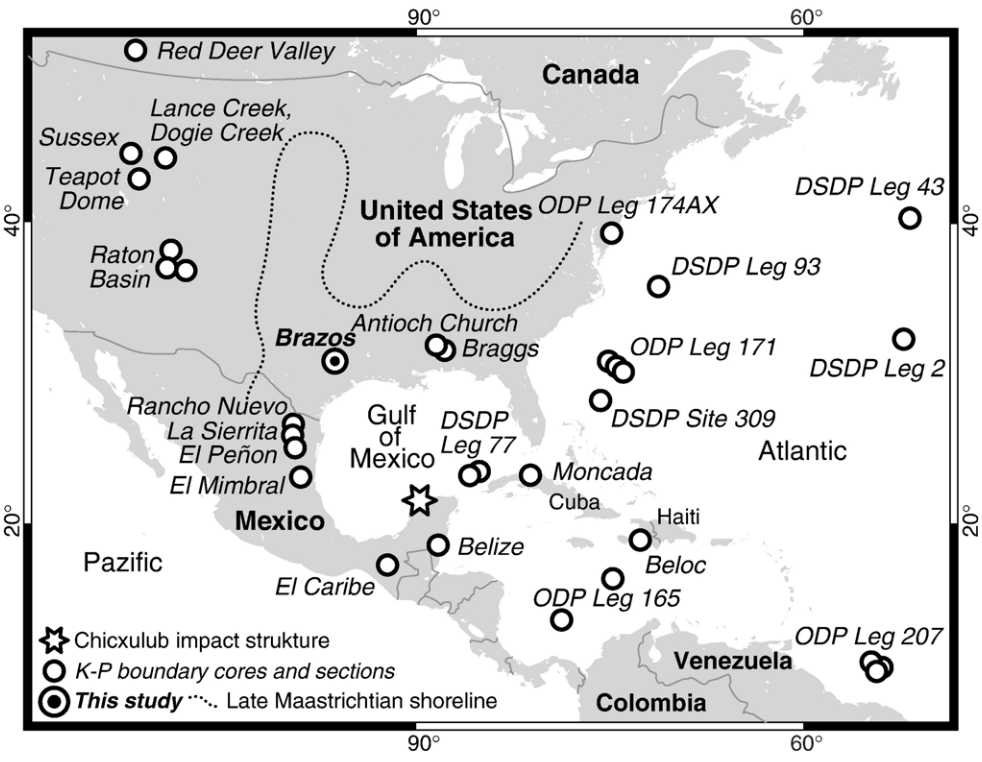

Fig. 1. Gulf of Mexico with adjacent areas and K–P boundary sections referred to in this study. Position of Latest Cretaceous shoreline and Western Interior Seaway according to Kennedy et al. (1998).

nesbeck et al., 1996), although most authors consider this deposit as tsunamite or tempestite genetically linked to the Chicxulub impact (Olsson and Liu, 1993; Smit et al., 1996; Schulte et al., 2003; Lawton et al., 2005).

Moreover, at Brazos, a distinct 10- to 25-cm-thick barren shale interval is 'sandwiched' between the Chicxulub ejecta and the first occurrence of Paleogene microfossils (Keller, 1989a; Gartner, 1996), similarly to the Yaxcopoil core from within the Chicxulub impact basin (see Goto et al., 2004; Keller et al., 2004; Smit et al., 2004). The stratigraphic position of this shale interval–whether it can be assigned to the late Maastrichtian or to the earliest Danian–is currently at issue.

Here, we provide an integrated study of the sedimentology, micropaleontology, mineralogy, geochemistry, and magnetic susceptibility from two cores drilled close to the famous Brazos River sections to address long- and short-term facies changes and depositional events. The rationale for our combined methodological approach was (i) to detect shifts in the position of the shoreline, (ii) to determine variations of the sediment provenance, and (iii) to assess paleoclimatic changes in the hinterland. In addition, this multidisciplinary approach also allows us to characterize the Chicxulub ejecta.

Preliminary data from the two Brazos cores published in Mai et al. (2003) and Schulte (2003) showed that the Brazos cores yielded no evidence for pronounced trans- or regressions until the early Danian, which shows a regressive event. Moreover, the Brazos cores yield a detailed record of Chicxulub ejecta and 1.6 m (!) of laminated dark shales between the Chicxulub ejecta- and mass extinction-horizon and the first appearance of Paleogene microfossils. However, correlation of the Chicxulub ejecta with K–P sections at greater distance to Chicxulub allows for unequivocally constraining the stratigraphic position of the 'sandwiched' shale unit as of earliest Danian age.

1.1. Locality and geological setting

The Brazos K–P outcrop area is situated along the Brazos River between Waco and Hearne (Figs. 1 and 2A) in south-central Texas. At present, some 15–20 Cretaceous–Paleogene outcrops and cores from the Brazos riverbed, the adjacent Cottonmouth Creek, and the Darting Minnow Creek are documented in the Brazos area (Fig. 2B and Hansen et al., 1987, 1993a,b; Yancey, 1996). The Brazos cores investigated for this study were drilled in close proximity at the western side of the Brazos River, about 370 m downstream from the Texas Highway 413 Bridge, which is located near the crossing between Texas Highway 413 and 1773 (Fig. 2B).

Paleogeographically, the Brazos area is located at the entrance to the Western Interior Seaway on the shallow northern Gulf of Mexico shelf (see Fig. 1 and Kennedy

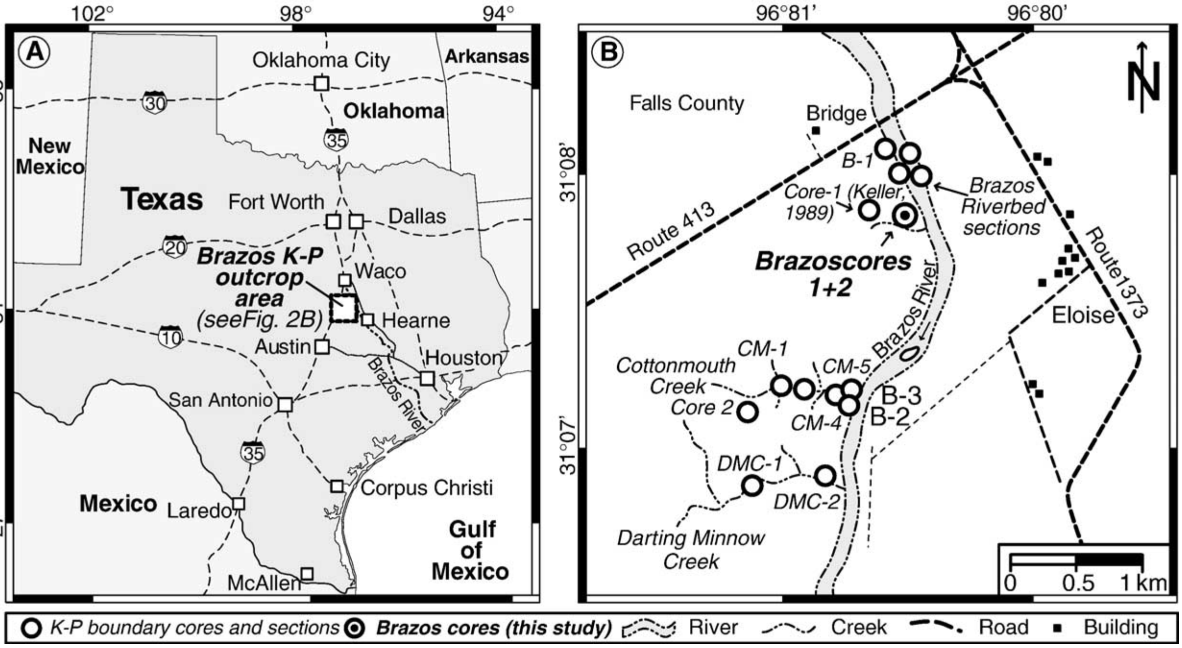

Fig. 2. (A) Map of Texas and (B) close-up of the Brazos area with the localities of outcrops and cores.

et al., 1998; Sweet and Braman, 2001). This region is known for nearly continuous, and predominantly siliciclastic sedimentation during the Late Cretaceous and the early Paleogene (Davidoff and Yancey, 1993). Quantities of sediment supply have generally been higher than the development of accommodation space on the continental shelf, resulting in an outward prograding shelf margin and an overall shallowing trend from the Latest Cretaceous to the late Eocene (Davidoff and Yancey, 1993). Therefore, marine sediments at the Brazos river site reflect a general trend from mid-to-outer shelf settings during the Latest Cretaceous–early Paleocene (shelf-slope break at approximately 100 km down-dip of the Brazos river outcrops) to a non-marine setting by the Eocene (basinward migration of the shelf-slope break). This general trend of environmental change in the Brazos area and the progradation of the Paleogene shelf margin has been modified substantially by variations in sediment supply and eustatic sea level (cf. Galloway, 1989).

1.2. Previous results from K–P studies at Brazos, Texas

Hansen et al. (1987) and Bourgeois et al. (1988) were the first to describe the sedimentology and the faunal patterns across the K–P boundary at Brazos, Texas. These studies revealed distinct sedimentary structures (“tsunamites or tempestites”) and an abrupt mass extinction at the K–P boundary that both were possibly related to an impact event —even long before the location of the K–P impact at Chicxulub had been found at around 1990 (Hildebrand et al., 1991). Based on foraminiferal data, however, Keller (1989a) and Keller and Stinnesbeck (1996) considered the K–P boundary sequence rather as sea-level lowstand deposit. In turn, subsequent sedimentological investigations by Smit et al. (1996) and Yancey (1996), further strengthened the case for impact-related tsunami or tempestite deposition at the K–P boundary. Consequently, both studies suggested that no major sea-level changes are detectable during this interval, besides a possible sequence boundary in the early Danian.

The most disputed “critical” interval of the Brazos K–P boundary, however, is the 15- to 25-cm-thick shale ‘sandwiched’ between the event deposit and the first appearance of Paleogene microfossils. High-resolution grain-size analysis by Smit et al. (1996) showed that this interval is normal-graded and hence, most likely reflects a short-term deposit from settling from the water-column. In spite of these detailed sedimentological studies, information about Chicxulub ejecta preserved in the event deposit has remained sparse. Preserved ejecta spherules are commonly of green color, hollow, and very fragile (Smit et al., 1996; Yancey, 1996) and sometimes even dismissed as glauconite grains (Keller and Stinnesbeck, 1996), whereas glassy ejecta particles have not been reported yet.

Magnetic susceptibility (MS) studies have not yet been conducted in the Brazos area, although a number of globally distributed K–P sections and cores have been investigated (e.g., Ellwood et al., 2003). Ellwood et al. interpreted the results of their measurements on cores from Oman, Italy, the Caribbean and the North Atlantic to show a common signal of regression across the K–P boundary immediately followed by a transgression. In addition, Herbert et al. (1995) and Herbert (1999) used the MS pattern and the sediment reflectance data to constrain the timing of the K–P boundary by incorporating Maastrichtian and Paleocene sedimentary (Milankovitch) cyclicity.

2. Methods

Optical microscopy of resin-stained thin sections was performed to assess the textural and mineralogical properties. For the mineralogical, geochemical, and magnetic analyses, samples were dried, crushed, and finely ground in an agate mill.

Samples were prepared for planktic foraminiferal biostratigraphic analysis at the University of Karlsruhe by using two size fractions (38–63 μm and >63 μm) after methods given by Pardo et al. (1996). The fraction >125 μm was used for qualitative and quantitative benthic foraminiferal analysis. For nannofossil biostratigraphy, sample material was ultrasonically cleaned at the University of Bremen in a weak ammonium solution for 3 min. The resulting suspension was allowed to settle for 3 min and the water decanted. The deposit was then again brought into suspension and a few drops spread over a graphitic scanning electron microscope (SEM) stub. After drying and coating with gold, the stub was observed in a SEM at 2500 magnification.

Non-clay and clay mineralogy was analyzed by X-ray diffractometry (XRD) at the Geological Institute of the University of Neuchâtel, with a SCINTAG XRD 2000 diffractometer and Cu-Kα-radiation. Diffractograms were evaluated with the MacDIFF software (freeware by R. Petschick, University of Frankfurt, see Petschick et al., 1996). In absence of a reliable internal standardization, the non-clay mineralogy is reported as counts per second. However, XRD analyses were conducted during one sample run to ensure the relative comparability of the data. The semiquantitative estimation of the relative abundance of the clay minerals (given in % of the clay fraction) was conducted by using the ratios of the weighted peak areas of smectite (weighting factor '1'), chlorite ('2'), illite ('4'), and kaolinite ('2') from glycolated specimens according to Biscaye (1965).

Major elements were determined by wavelength-dispersive X-ray fluorescence spectrometry (WDS) at the Institute for Mineralogy and Geochemistry, University of Karlsruhe, with a SRS 303 AS XRF. For these analyses, fused glass discs were prepared from a mixture of 1 g ignited powder of each sample and 4 g of SPECTROMELT. Major elements were evaluated by a fundamental parameter calibration procedure. Trace elements (Cr, Ni, Cu, Zn, As, Rb, Sr, Y, Zr, Ba, La, Ce, and Pb) were analyzed from bulk powder samples (5 g) by energy-dispersive X-ray fluorescence spectrometry (EDS) with a SPECTRACE 5000 X-ray analyzer at the same institute. Trace elements were determined using a Compton and intensity matrix correction procedure. Detailed analytical procedures, detection limits, and standards used were compiled by Kramar (1997).

The magnetic susceptibility (MS) was determined at the magnetic laboratory of the University of Heidelberg in low fields (300 A/m, 920 Hz) with a Kappabridge KLF-3 (AGICO). Three aliquots with 7 g bulk powder of every sample were measured and a mean value calculated.

Wavelength-dispersive (WDS) and energy-dispersive (EDS) electron microprobe analyses (EMPA), as well as back-scattered electron (BSE) images were performed with a CAMECA SX50 microprobe on polished, carbon-coated thin sections at the Laboratory for Electron Microscopy, University of Karlsruhe. Quantitative (WDS) microprobe analyses were carried out using the crystals TAP (Si, Al), PET (Ti, Ca, K), RAP (Mg, Na) and LiF (Fe, Mn). All quantitative major element analyses were calibrated with the following standards: Fe: Fe_2O_3; Si: wollastonite; Mg: MgO; K: orthoclase; Ca, Al: anorthite; Ti: $MnTiO_3$; Na: albite. Accelerating voltage was set to 15–20 kV with a primary beam of 15 nA; counting times of 20–40 s were used per element. Detection limits are in the range between 0.5 and 1 wt.%. Oxide percentages were calculated using a ZAF correction program (Fialin, 1988).

3. Results and interpretation

3.1. Lithostratigraphy and sedimentology

The detailed lithology of the two Brazos cores as well as the subdivision of the Brazos K–P interval into the corresponding lithological units 'A' to 'I' of Hansen et al. (1987, 1993a) is shown in Fig. 3. The K–P event deposit is outlined in Fig. 4 that also includes the lithological units 'BCB' to 'RPH' introduced by Yancey (1996).

3.1.1. Corsicana Formation (Unit A)

The Corsicana Formation (Unit A) comprises the lower 0.8 and 6.7 m of cores 1 and 2, respectively, and consists of friable dark grey–brown shale, which is slightly laminated. The Corsicana shales include shell hash and small mollusks; evidence for bioturbation is rare. In both cores, the 20- to 40-cm-thick topmost interval of these shales is devoid of lamination and strongly disturbed. **Unit A** is interpreted as 'mud' deposited between, or slightly below, fair-weather and storm wave base; storm-driven currents probably led to intermittent reworking of shells (Hansen et al., 1987, 1993b; Kerr and Eyles, 1991). However, no distinct sand- or silt-layers have been observed, suggesting that reworking by currents acted on a local scale. The lamination of the shales may record subtle changes in the texture and discharge of suspended sediment or may be a later, diagenetic texture (Schieber, 1998).

3.1.2. Littig member of the Kincaid Fm. (Unit B–I)

The Corsicana Fm. is disconformably overlain by the Littig Member of the Kincaid Formation (Yancey, 1996). The basal part of the Littig Member is a 0.2- to 0.4-m spherule-rich, sandy–silty, and carbonate-rich sequence, commonly referred to as "K–P event deposit", which comprises Units B to F.

The basal **Unit B** (BCB, basal conglomerate bed) is a 10-cm-thick brown, disturbed shale with cm-sized shale clasts. It is rich in shell hash and shows no lamination. The sedimentologic characteristics of Unit B meet the criteria suggested by various authors to be indicative of an origin from a debris flow (e.g., Iverson, 1997; Mulder and Alexander, 2001). Yancey (1996) has drawn a similar conclusion for the basal part of the Brazos event deposit.

Unit C (SCB, spherulitic conglomerate bed) is a 8-cm-thick, normal-graded spherule-rich layer, speckled with green, black, red, white, grey mm-sized ejecta–spherules. However, this unit lacks bedding and sorting characteristics typical of primary fallout deposition (e.g., Fisher and Schmincke, 1984; Bitschene and Schmincke, 1991), but shows characteristics of deposition from grain-dominated debris flows with decreasing current energy (e.g., Iverson, 1997; Mulder and Alexander, 2001), in line with the interpretation of Yancey (1996).

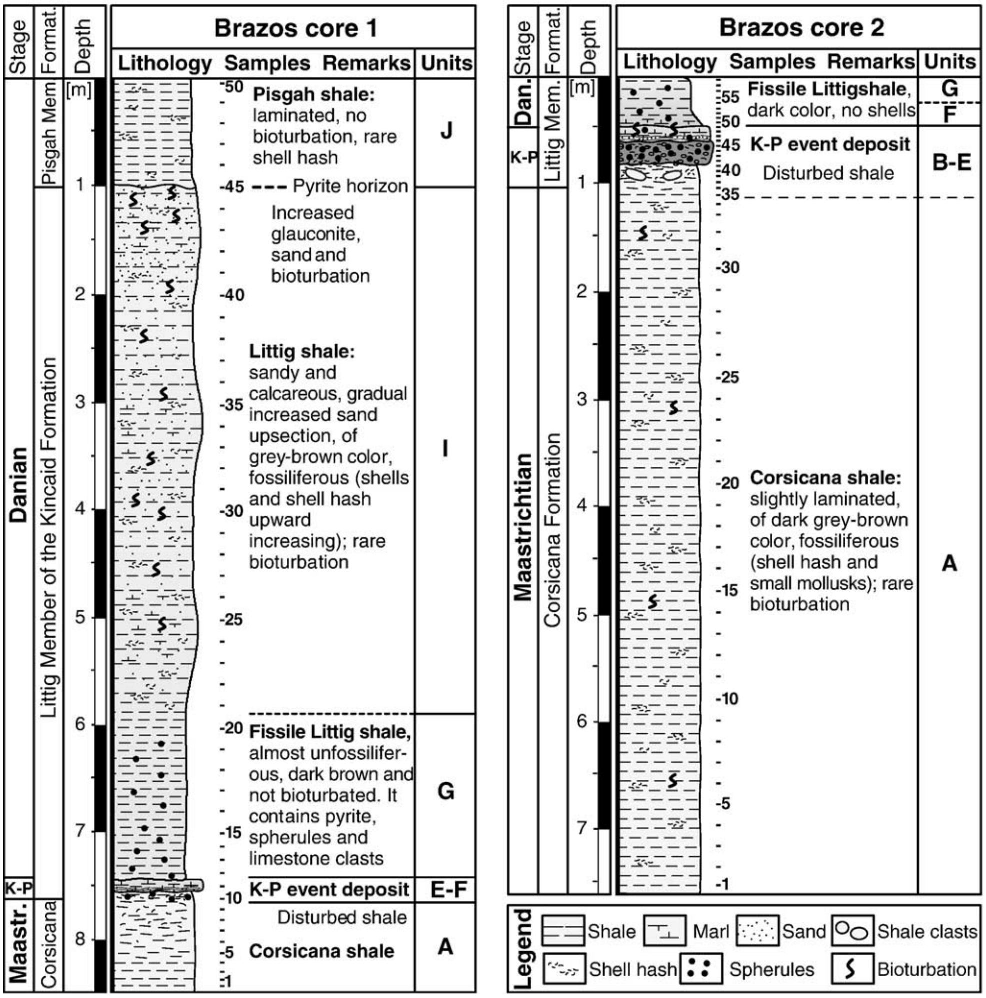

Fig. 3. Stratigraphy and lithology of (A) Brazos core 1 and (B) Brazos core 2.

Unit D (GSB, granular sand bed) consists of 0.5- to 1-cm-thick thin silty–sandy layers that are intercalated in the upper part of Unit C and lower part of Unit E. The spherules, limestone clasts (accretionary lapilli), shale clasts, phosphatized particles, and sand-sized carbonate-rich material in Unit C, as well as the thin intercalated layers of micaceous silt–sand grains of Unit D, suggest that a mixture of materials from different source areas occurred: (i) ejecta spherules, derived via air–water fallout from the Chicxulub impact in southern Mexico, (ii) silt–sand, originated from more proximal coastal areas, and (iii) phosphatized particles, which derived either by winnowing and lateral reworking of adjacent unconsolidated sediments or lag horizons (Schieber, 1998).

Unit E (HCS, hummocky sandstone unit) is a 10-cm-thick package of alternating layers of light grey, silty, and calcareous sands. These layers show planar lamination and low amplitude wavy bedding; in the upper part, more pronounced asymmetric current ripples are present. This unit contains some spherules, rusty concretions and *Ophiomorpha* or *Thalassinoides* burrows with diameters of 0.5–1 cm. The sedimentological features of Unit E, with the intercalated layers of Unit D, mark a change of the hydrodynamic conditions, compared to the underlying units, implying deposition from suspension during multiple subsequent steps of waning current energy (upper to lower flow regime, see Shanmugam, 1997; Shiki et al., 2000). The burrows in this unit are confined to the topmost part of the sequence and–as indicated by the dark mud infill– apparently originated from a horizon of different sediment composition.

Unit F (CCH, calcareous clayey bed) is a 6-cm-thick, massive, and indurated calcareous marl that grades upward into Unit G. It shows no bioturbation

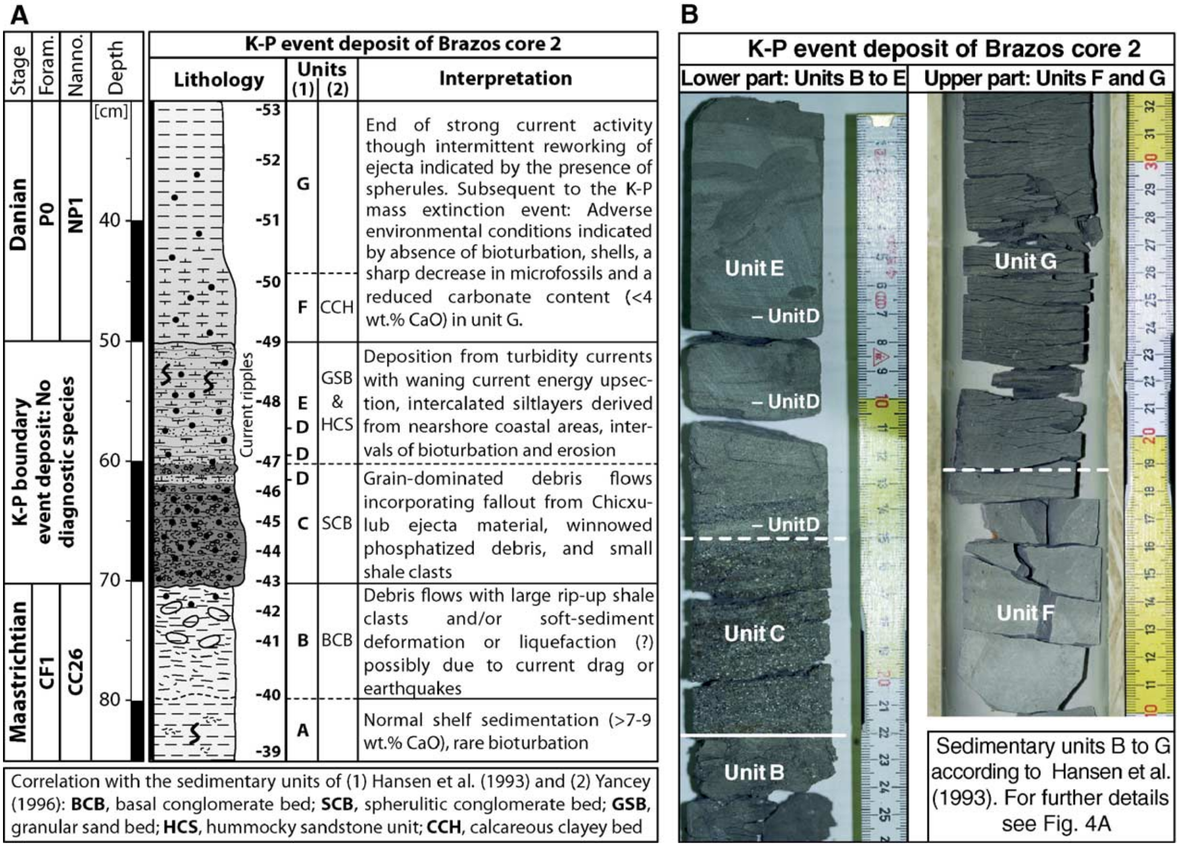

Fig. 4. (A) Detailed lithology and subdivision of the K–P event deposit in Brazos core 2 combined with the lithological units provided in Hansen et al. (1993b) and Yancey (1996). (B) Photographs showing the K–P event deposit in Brazos core 2 (units B to F) and the gradual transition to the overlying carbonate-poor unit G.

or lamination; some spherules, limestone clasts and rusty concretions as well as pyrite are present. Unit F may represent fine-grained carbonaceous ejecta material, although no particular smectite enrichment was encountered in this layer. Alternatively, this limestone is made of inorganically precipitated micrite, since it contains only few microfossils and no evidence for particular nannofossil blooms (see also Bralower et al., 2002).

The part of the Littig Member above the "K–P event deposit" comprises Unit G to Unit I (Fig. 3). **Unit G** is 1.6 m (core 1) and 0.5 m (core 2) fissile and laminated, almost unfossiliferous dark brown clayey shale (Unit G). Unit G contains pyrite and rusty concretions, as well as altered spherules and carbonate chips. This shale is generally devoid of fossils and shows no bioturbation. The sporadic occurrence of altered spherules, as well as limestone clasts throughout this interval, indicates intermittent periods of reworking and redeposition. The absence of bioturbation may also suggest rapid sedimentation and reworking (Brett and Allison, 1998). **Unit H** is a cm-thick sandy layer that is intermittently present in some Brazos outcrops above the event deposit, although it was not observed in the Brazos cores of this study. **Unit I** conformably overlies Unit G and is about 6 m thick in Brazos core 1. This unit is carbonate-rich sandy–silty shale of light grey color with upward-increasing bioturbation, carbonate and shell content. The uppermost meter of Unit I is sandier, contains some glauconite, and is bioturbated by cm-thick *Thalassinoides* burrows (MSB or DSB, middle or dirty sandstone bed). Its top is a pyrite- and iron oxide-rich layer (RPH, rusty pyrite concretion horizon). Unit I may record the return to normal sedimentary conditions almost equivalent to Unit A, although the increased coarse detritus content suggests a more proximal facies (MacQuaker et al., 1998).

3.1.3. Pisgah member of the Kincaid formation (Unit J)

The Pisgah Member comprises the topmost part of core 1 and consists of slightly fossiliferous brown shale (with shell hash, small mollusks, sea-urchin spines), which is moderately bioturbated and in part laminated. The absence of coarse detritus compared to the underlying indicates an abrupt change to a more distal setting (MacQuaker et al., 1998).

3.2. Biostratigraphy and paleoecology

The preservation of coccoliths and foraminifera in the Brazos cores is excellent, facilitating a detailed biostratigraphical and paleoecological analysis (Fig. 5). Only microfossils from the K–P event deposit are rare and likely reworked, hence the units B–F are excluded from the biostratigraphic analysis. The biozonation is based on the schemes provided by Martini (1971) and Perch-Nielsen (1985) for calcareous nannofossils and Berggren et al. (1995) for planktic foraminifera with added refinements for the Late Cretaceous zonation by Pardo et al. (1996).

3.2.1. Calcareous nannofossils

The calcareous nannofossils in the interval from the lower part of Brazos core 1 and core 2 up to the event deposit shows a stable, very diverse (~45 species) latest Maastrichtian assemblage of the *Micula murus* zone (CC26). The index fossil for the latest Maastrichtian subzone CC26b, *Micula prinsii* (Self-Trail, 2001), was not detected during this study. This designation agrees with previous studies by Jiang and Gartner (1986), although these authors reported the intermittent and very rare occurrence of *M. prinsii* concomitant to the occurrence of *M. murus* throughout the 18 m below the K–P event deposit. The finding of single occurrences of Paleogene coccoliths (and foraminifera) below the event deposit in the Brazos outcrops by Montgomery et al. (1992) have not been confirmed by other biostratigraphic studies (e.g., Olsson and Liu, 1993), including ours. However, related to recent observations by Mai et al. (2003) from the Antioch Church core (Alabama), El Kef (Tunisia), and Geulhemmerberg (The Netherlands), tiny specimens of *Neobiscutum romeinii*, *Neobiscutum parvulum*, and *Cruciplacolithus primus* have also been observed in the first sample of core 2, about 8 m below the event deposit. These calcareous nannofossils have long been used as index fossils for the earliest Paleogene, although recent studies show their consistent presence already in latest Maastrichtian sediments during the uppermost part of the *M. murus* Zone (CC26, Mai et al., 2003). At the Elles K–P section, Tunisia, their first occurrence roughly parallels the first occurrence of *M. prinsii* (Gardin, 2002).

In the 1.6-m-thick interval (Unit G) above the K–P event deposit, the abundance of calcareous nannofossils and their species number is drastically reduced. The remaining nannofossils constitute an impoverished Late Cretaceous fauna; exclusively Paleocene species were not observed. Jiang and Gartner (1986) encountered similar findings, although they figured a nannofossil-poor interval overlying the event deposit of only about 20–30 cm in thickness. A similar drop in abundance of calcareous nannofossils has been observed frequently above the K–P boundary (e.g., at El Kef, Tunisia), preceding the first occurrence of Paleogene species (Gartner, 1996; Pospichal, 1996a).

The first definite Danian calcareous nannofossil *Biantholithus sparsus* occurs at 1.6 m above the event deposit in core 1; Brazos core 2 yielded no Danian species. The presence of *B. sparsus* in Brazos core 1 suggests a zone NP1 age for the sediments above Unit G. In addition, abundant (reworked?) Cretaceous species, blooms of *Operculodinella operculata* (*Thoracosphaera operculata*, a calcareous dinoflagellate cyst) and *Braarudosphaera bigelowii* are present. In the interval above the *T. operculata* and *B. bigelowii* blooms, acmes of *N. romeinii* followed by *N. parvulum* are concomitant to an upward decreasing number of reworked Cretaceous species. A bloom of *C. primus* follows the acme of *N. parvulum*. The uppermost meter of Brazos core 1 is marked by an acme of *Futyania petalosa* with only a few reworked Cretaceous coccoliths. The index marker of the *Cruciplacolithus tenuis* Zone (NP2) was not observed, although the acme of *F. petalosa* is characteristic for the upper part of Zone NP1 and the lower part of Zone NP2.

An ordered succession of opportunistic blooms following the first appearance of Paleogene calcareous nannofossils is a characteristic feature of Zone NP1 in many K–P boundary sections (Gartner, 1996; Gardin and Monechi, 1998; Gardin, 2002). A remarkably similar succession of calcareous nannofossil acme-subzones has been obtained for the Brazos section by Jiang and Gartner (1986), and for the Elles section, Tunisia, by Gardin (2002). However, the blooms of *B. bigelowii* and *N. romeinii* are contemporaneous to planktic foraminifera Zone P0 at the Brazos core 1 (see below), and occur generally above Zone P0 in several K–P sections elsewhere (e.g., Tunisia, Italy, Spain, see Gartner, 1996; Gardin and Monechi, 1998; Gardin, 2002).

3.2.2. Planktic foraminifera

Planktic foraminifera in the basal part of core 2, up to 0.5 m below the event deposit, represent an impoverished Maastrichtian assemblage with a low number of species. This fauna is largely dominated by heterohelicids and guembelitrids with subordinate hedbergellids and globigerinoids, as well as very rare *Globotruncana* and *Rugoglobigerina*. No index foraminifera for the late(est) Maastrichtian have been encountered (e.g., *Abathomphalus mayaroensis* or *Plummerita hantkeninoides*). *Gansserina gansseri* is a common species in the Corsicana Fm. of Texas (Smith and Pessagno, 1973), but is absent in our samples. This suggests that the studied interval corresponds to Zone CF2, since this zone is defined by the interval between the last appearance date (LAD) of *G. gansseri* at the top of the *Pseudoguembelina hariaensis* Zone (CF3), and the first appearance date (FAD) of *P. hantkeninoides* or *Plummerita reicheli*, which both mark the latest Maastrichtian Biozone CF1 (Pardo et al., 1996). The upper 0.5 m of the Corsicana Fm. contained a few specimens of *P. reicheli* indicating the uppermost Maastrichtian Zone CF1. The planktic foraminifera data are consistent with previous results from Keller (1989a,b), who reported the presence of an impoverished latest Maastrichtian foraminiferal fauna below the event deposit in combination with the general absence of *A. mayaroensis*. However, Keller (1989a, Fig. 9) reported the sporadic occurrence of *P. reicheli* in an interval extending 24 m below the K–P event deposit, even paralleling the occurrence of *G. gansseri* (Zone CF3 of Keller et al., 1995). In other upper Maastrichtian sections (e.g., at Caravaca, Spain), however, *P. reicheli* is observed at several meters below the K–P boundary (Zone CF1), well above the last occurrence of *G. gansseri* (Pardo et al., 1996).

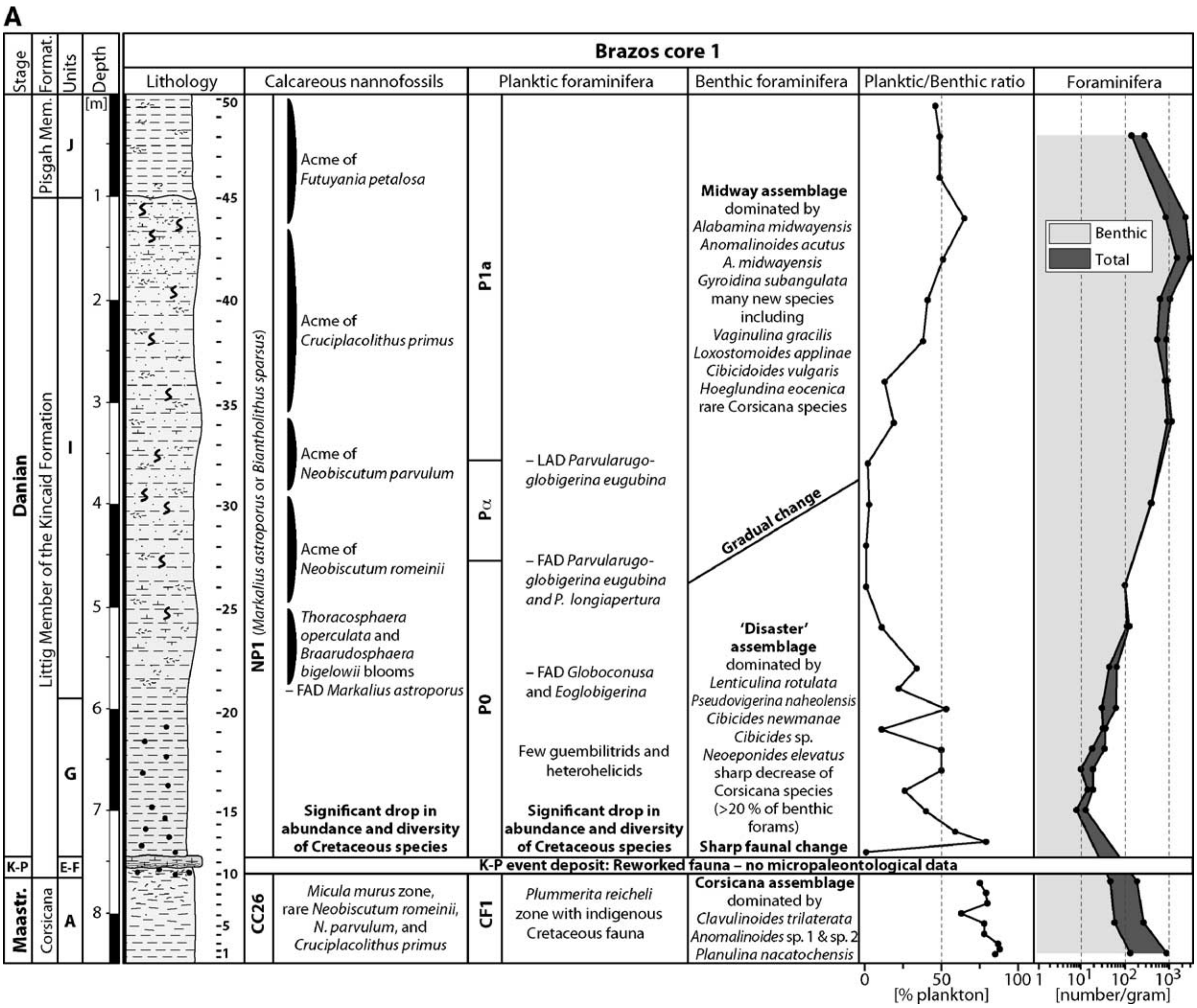

Fig. 5. Calcareous nannofossils and planktic/benthic foraminifera and biostratigraphy of (A) Brazos core 1 and (B) Brazos core 2. A legend is provided in Fig. 3.

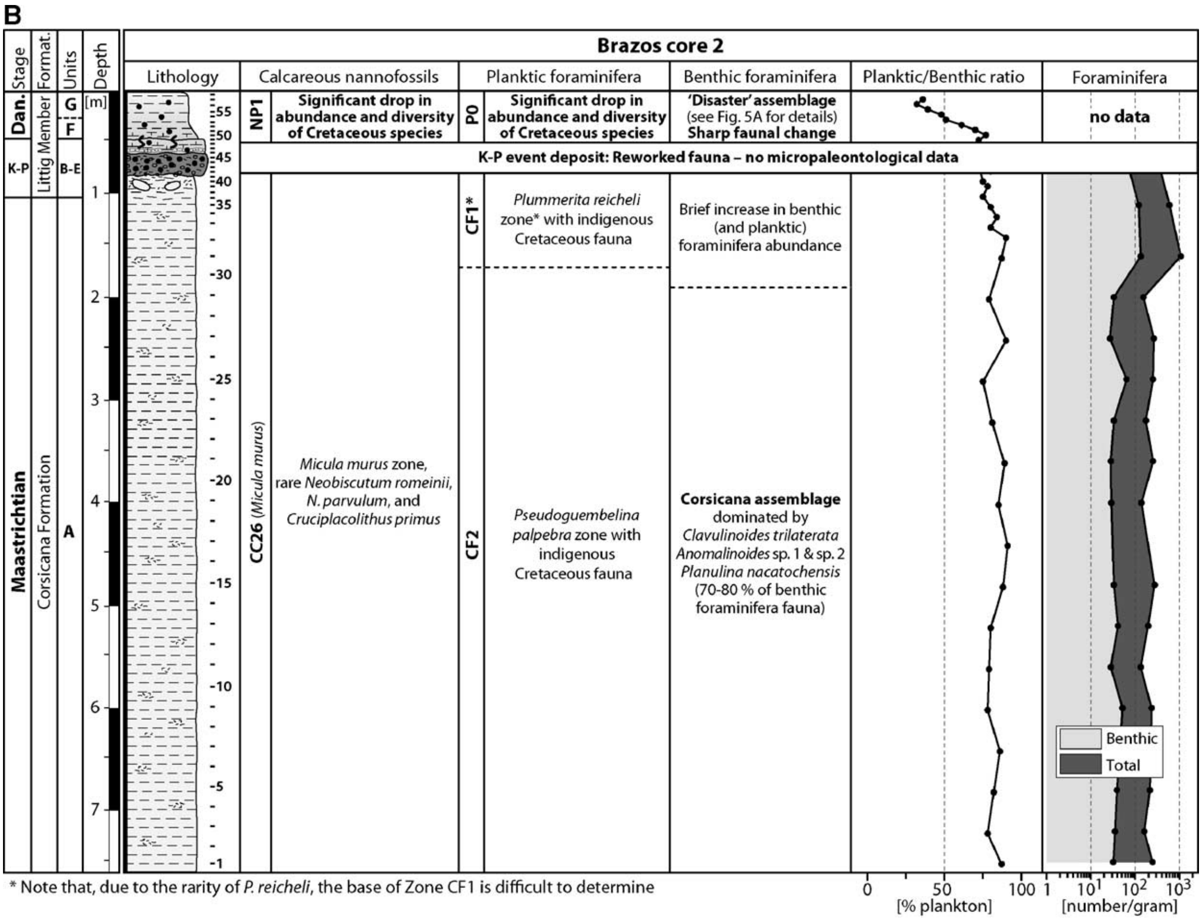

Fig. 5 (*continued*).

Planktic foraminifera in Unit G are rare and mainly consist of guembelitrids and heterohelicids. No index species have been detected. These planktic foraminifera data are well comparable to previous findings of Keller (1989a,b), although the FAD of Paleocene species is about 25 cm above the event deposit in the Brazos core studied by Keller, which is much lower than the 1.6 m in the Brazos core 1 of this study.

The earliest (38–63 μm) Paleocene planktic foraminifera, including *Globoconusa* and *Eoglobigerina,* which are indicative of Zone P0, are present about 1.6 m above the event deposit in core 1. In addition, rare rugoglobigerinids and heterohelicids occur in this interval. The first occurrence of *Parvularugoglobigerina eugubina* and *Parvularugoglobigerina longiapertura* at 20–40 cm above the base of Zone P0 marks the beginning of Zone Pα (Berggren et al., 1995) or P1a (Keller et al., 1995). However, *Parasubbotina pseudobulloides* was not found and therefore, it was not possible to subdivide Zone P1a into P1a(1) and P1a(2), based on the FAD of this species (Keller et al., 1995). The absence of *P. eugubina* in the topmost 3.6 m of core 1 suggests a Zone P1a (Berggren et al., 1995), or P1b (Keller et al., 1995) age for this interval.

In conclusion, the biostratigraphy from planktic foraminiferal and calcareous nannofossil allows for a relatively imprecise Maastrichtian zonation and for a detailed zonation of the Danian. The thicknesses and durations of the zones and the calculated sedimentation rates are shown in Table 1.

Table 1
Overview on thickness of planktic foraminiferal zones, their estimated duration and the calculated sedimentation rates for the Brazos cores

Biozone	Thickness	Duration[a]	Sedimentation rate
P1a	At least 3.5 m	300 ka	At least 1.2 cm/ka
Pα	1 m	200 ka	0.5 cm/ka
P0	3 m	20–40 ka	750 cm/ka
CF1–CF2	At least 6.8 m	450 ka	At least 1.25 cm/ka

[a] Duration according to Berggren et al. (1995), Cande and Kent (1995) and Pardo et al. (1996).

3.2.3. Benthic foraminifera

The benthic foraminiferal Corsicana assemblage (Unit A) is dominated by *Clavulinoides trilatera*, *Anomalinoides* sp. 1 and sp. 2 and *Planulina nacatochensis*, together consistently constituting 70–80% of the benthic assemblage (size fraction >125 μm). This late Maastrichtian benthic fauna is stable up to the base of the K–P event deposit, with few first or last appearances. Planktic/benthic (P/B) ratios vary between 75 and 90% plankton, but remain high and stable up to the top of the Corsicana Fm. The only foraminiferal parameter showing significant temporal variation is the number of foraminifera per gram of dry sediment. For most of the Maastrichtian record the total number of foraminifera (>125 μm) is ~200 specimens/gram sediment. The topmost 50 cm of the Corsicana Fm., however, shows an increase up to 300–1000 specimens/g.

The K–P event deposit marks an abrupt faunal change in the benthic foraminiferal assemblage. The post-event ("disaster") assemblage in Unit G and in the lower part of Unit I constitute a new fauna with a subordinate component of Corsicana taxa. The four most common Corsicana taxa compose between 1% and 18% of the new benthic fauna. *Pseudouvigerina naheolensis* is the first new species to appear, composing up to 42% of the assemblage. It is followed by other common species such as *Eponides elevatus*, *Cibicides newmanae*, and *Cibicides* sp. 1. P/B ratios in this interval gradually drop from a peak value of 80% plankton just above the K–P event deposit to below 5% plankton in the lower part of Unit I. It is striking that within this interval there is a one-to-one match with samples that contain a relatively large proportion (8–18%) of Corsicana benthic taxa. This relationship strongly suggests that a significant proportion of both foraminifera groups within this interval is reworked. At the same time, the total number of foraminifera is extremely low in the lower part of Unit G (~20 specimens/gram), but gradually increases to 100 specimens/g in the lower part of Unit I.

With the appearance of the benthic taxa *Alabamina midwayensis* and *Anomalinoides midwayensis* during Zone Pα–P1a, a typical benthic "Midway-fauna" (Berggren and Aubert, 1975) was established; other common taxa are *Anomalinoides acutus* and *Gyroidina subangulata*. Only a few other species, for instance *Pulsiphonina prima*, *Cibicidoides alleni*, and *Lenticulina rotulata*, are observed in this interval. Individual scattered single specimens of the Corsicana taxa are observed within this Midway assemblage, suggesting that there was limited – if any – reworking from the upper Maastrichtian into this interval.

The gradual formation of the Midway assemblage coincides with increasing P/B ratios, up to 50% plankton and increasing foraminiferal numbers up to a maximum of 3000 specimens/g at the top of the Littig Member. The latter values drop again in the Pisgah Member. The Midway fauna typifies deposition in middle to outer shelf setting (50–100 m). The other assemblages are not well known and thus their paleobathymetric indication is unclear. However, judging from the higher P/B ratios of the Corsicana Fm., it can be concluded that deposition during the latest Maastrichtian occurred on a deeper part of the shelf (~100 m). It is, however, difficult to assess the depositional conditions during the earliest Paleocene (Zones P0 and Pα) by evaluating P/B ratios since most planktic foraminifera became extinct within this interval and the ones present are probably reworked.

3.3. Mineralogical phases

The bulk-rock mineralogy of marine sediments–especially the calcite/siliciclastic detritus ratio–can be used to detect changes in terrigeneous input and in biogenic productivity that both can ultimately be related to transgressive–regressive events. Similarly, clay mineral assemblages change with increasing distance from the shoreline (e.g., Chamley, 1997; Bengtsson and Stevens, 1998; Schutter, 1998). Therefore, both bulk-rock and clay mineralogy may give evidence of relative sea level changes within a sequence stratigraphic framework. On the other hand, inherited clay mineral assemblages in marine sediments record the climate conditions in the hinterland (e.g., Gingele, 1996; Yuretich et al., 1999; Müller et al., 2001), although careful consideration of the facies evolution, the regional setting, and possible source regions is mandatory (e.g., Deconinck et al., 2003; Thiry, 2000).

The non-clay minerals identified in the bulk powder fraction include quartz and calcite, with minor amounts of K-feldspar (Fig. 6). Plagioclase and pyrite, as well as accessory hematite is also present in low quantities (see details in Schulte, 2003). Plagioclase is dominant over K-feldspar in most samples. In the late Maastrichtian interval below the K–P event deposit, calcite is remarkably constant and only shows a slight increase in the uppermost part, together with an increase in the amount of foraminifera and shell hash. The other non-clay phases reveal only insignificant fluctuations and no apparent long-term trends. The

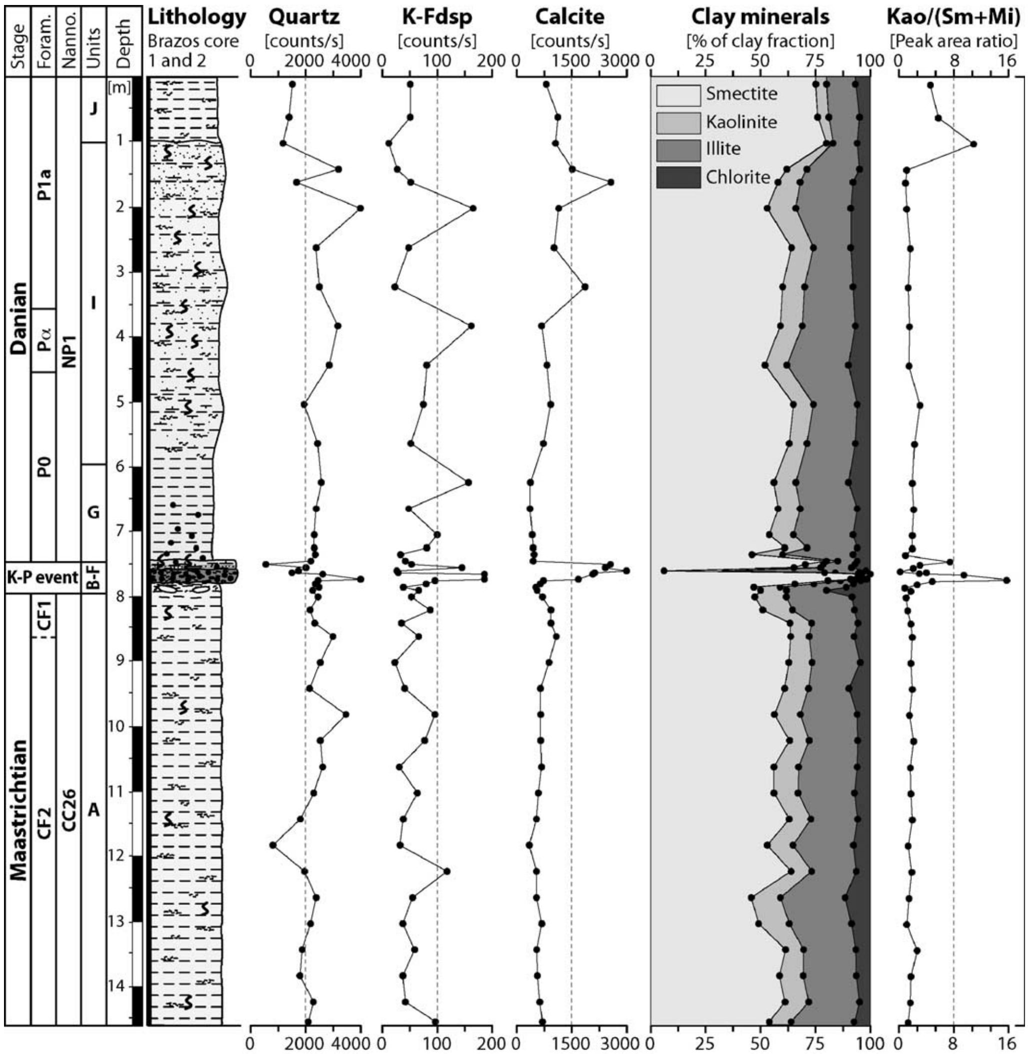

Fig. 6. Composite illustration of the non-clay and clay minerals of the two Brazos cores as determined from X-ray diffractometry. Non-clay minerals are given in counts per second, whereas clay mineral data is given in relative percent of the clay fraction with correction factors (Biscaye, 1965). In addition, the carbonate/detritus and the smectite/(kaolinite + illite + chlorite) ratios are shown. A legend is provided in Fig. 3.

K–P event deposit is characterized by an abrupt increase of calcite (doubling of counts per second) and pyrite, concomitant to a decreased quartz and plagioclase content. Above the event deposit, in the carbonate-poor shale, abundances of mineral phases step back to 'pre-event values', although calcite shows slightly lower values and pyrite increases significantly. The calcite, quartz and feldspar content between the base of the earliest Danian and the pyritized horizon is strongly fluctuating with high peak values. In the uppermost meter of Brazos core 1, above the pyritized horizon, the contents of calcite, quartz, and feldspar decrease abruptly.

The clay mineral assemblage of both Brazos cores is characterized by strong predominance of smectite, which comprises generally about 50–75% of the clay fraction (Fig. 6). Additional components include illite (~20%) and about equal amounts of chlorite and kaolinite (5–15%, each). Mixed layer clay minerals, for instance illite–smectite, illite–chlorite, and chlorite–smectite, are generally below 5% and have therefore not been included in the quantitative analysis. The variations in relative abundance of clay minerals in the Brazos cores reveal that there are no substantial long-term changes in the clay mineral composition as, from a quantitative and qualitative point of view, the clay mineral assemblage of late Maastrichtian and early Danian shales is quite similar. There are only subtle fluctuations in the range of ±5–10%, which is well within the error range of the methodology used

(Petschick et al., 1996). Significant short-lived changes, however, are associated (i) with the K–P event deposit, which shows a prominent 10–20% smectite detriment in its lower part and a strong increase of smectite decrease in its upper part (up to 95%), and (ii) with Unit I, which reveals an increased smectite content, compared to the underlying unit.

The smectite of the Corsicana and Kincaid Formation generally shows medium- to well-defined peaks with a crystallinity index ("FWHM", full width at half maximum peak height above background, Moore and Reynolds, 1997) of about 1°–1.3° 2θ, indicating a certain degree of disorder, typical for detrital smectites. Deviations from these crystallinity values occur in the K–P event deposit–specifically in Unit D–where lower crystallinity index values (FWHM ~0.6° to 0.8° 2θ) imply a significant higher crystallinity and may suggest that a large part of this smectite formed as an authigenic phase by the alteration of glassy ejecta material.

Additional constrains on the qualitative classification of the smectites comes from their (060) reflections in bulk rock powder samples (Moore and Reynolds, 1997). The smectite in the shale above and below the K–P event deposit is characterized by (060) peaks in the range between 61.6° and 62.3 °2θ, indicative of dioctahedral smectites (e.g., montmorillonite). In contrast, samples from the event deposit show prominent peaks at about 60.9° and 61.2° 2θ, which may indicate the presence of nontronite and/or saponite (Moore and Reynolds, 1997), as also revealed by EMP analysis (see Section 3.6).

3.4. Major and trace element stratigraphy

According to studies by Keller et al. (1998b), Jarvis et al. (2001), and Müller et al. (2001), variations of geochemical phases may provide an objective tool at hand to trace even subtle lithofacies changes and, therefore, paleoenvironmental changes within a sedimentary succession. This can be conducted by monitoring elements related to biogenic productivity (e.g., Ca, Sr, Ba, P) versus elements typically associated with terrigeneous detritus (e.g., Al, Rb, Zr, Ti, see Jeans et al., 1991; Wray and Gale, 1993; Müller et al., 2001; Kastner, 2003). Moreover, geochemical criteria for identifying systems tracts and proximal–distal facies trends (for instance the Si/Al, Si/Ca and Zr/Rb ratio), which ultimately may be related to relative sea level, have been proposed (e.g., Jarvis et al., 2001). For instance, zirconium (Zr) is commonly enriched in heavy minerals and hence associated with the relative coarse-grained fraction of fine-grained siliciclastic sediments, whereas rubidium (Rb) in fine-grained siliciclastic rocks is associated with the clay minerals and the micas (Dypvik and Harris, 2001). In consequence, the Zr/Rb ratio may be used to trace grain size variations of the sediments, with higher values in the relatively coarser units and vice versa. In contrast, strontium (Sr) is normally associated with carbonate minerals (Elderfield et al., 1996); only a small amount of Sr may also be associated with feldspar and biotite. The (Zr+Rb)/Sr ratio commonly reflects the balance between clastic and carbonate contents with high values typically found in samples with little calcium carbonate.

Selected geochemical data from analyses performed on both Brazos cores are presented in Fig. 7. The element abundances throughout the lower 3 m of Brazos core 2 show only insignificant fluctuations and no distinct compositional changes occur, as sustained by constant element/Al, Sr/Ca, and Zr/Ti ratios. Above the relative uniform basal part of the Brazos core 2, the 1-m-thick interval immediately below the K–P event deposit shows slightly increasing contents of CaO and Sr as well as reduced Sr/Ca ratios. The spherule-rich bed has an amplified carbonate and Sr content concomitant to strong depletion of all other elements, whereas the ratios of Si, Ti, Fe, and Mg against Al increase. This interval also shows an abrupt lowering of the Sr/Ca ratio.

All elements and element ratios decrease gradually to pre-event values in the upper part of the event deposit and in the capping marl layer. The carbonate-poor, 1.2-m-thick shale interval above the event deposit, shows a >50% drop of the carbonate contents and a twofold increase of the Sr/Ca ratio, when compared to the late Maastrichtian shales below the event deposit. Concomitant to this decrease in carbonate content, geochemical phases associated with terrigeneous detritus (e.g. Al, Ti) show slightly higher quantities than in the marls below the event deposit. In the upper part of the carbonate-poor interval, the shales become gradually enriched in carbonate. Concomitant to the first appearance of Paleocene microfossils and to the onset of sequential calcareous nannoplankton blooms during Zone P1α and NP1, a series of carbonate maxima (CaO >20 wt.%) occurs. In the upper 2 m of this interval (1 to 3 m core depth), the Si/Al ratio is considerably higher, although other detrital phases (e.g., Ti, Rb) are not elevated, pointing to increased input of silica-rich phases (e.g., quartz). An iron oxide- and pyrite-rich layer (>20 wt.% FeO) marks the top of this interval. In the topmost meter of Brazos core 1–above the pyrite-rich horizon – the Si/Al ratio decreases substantially,

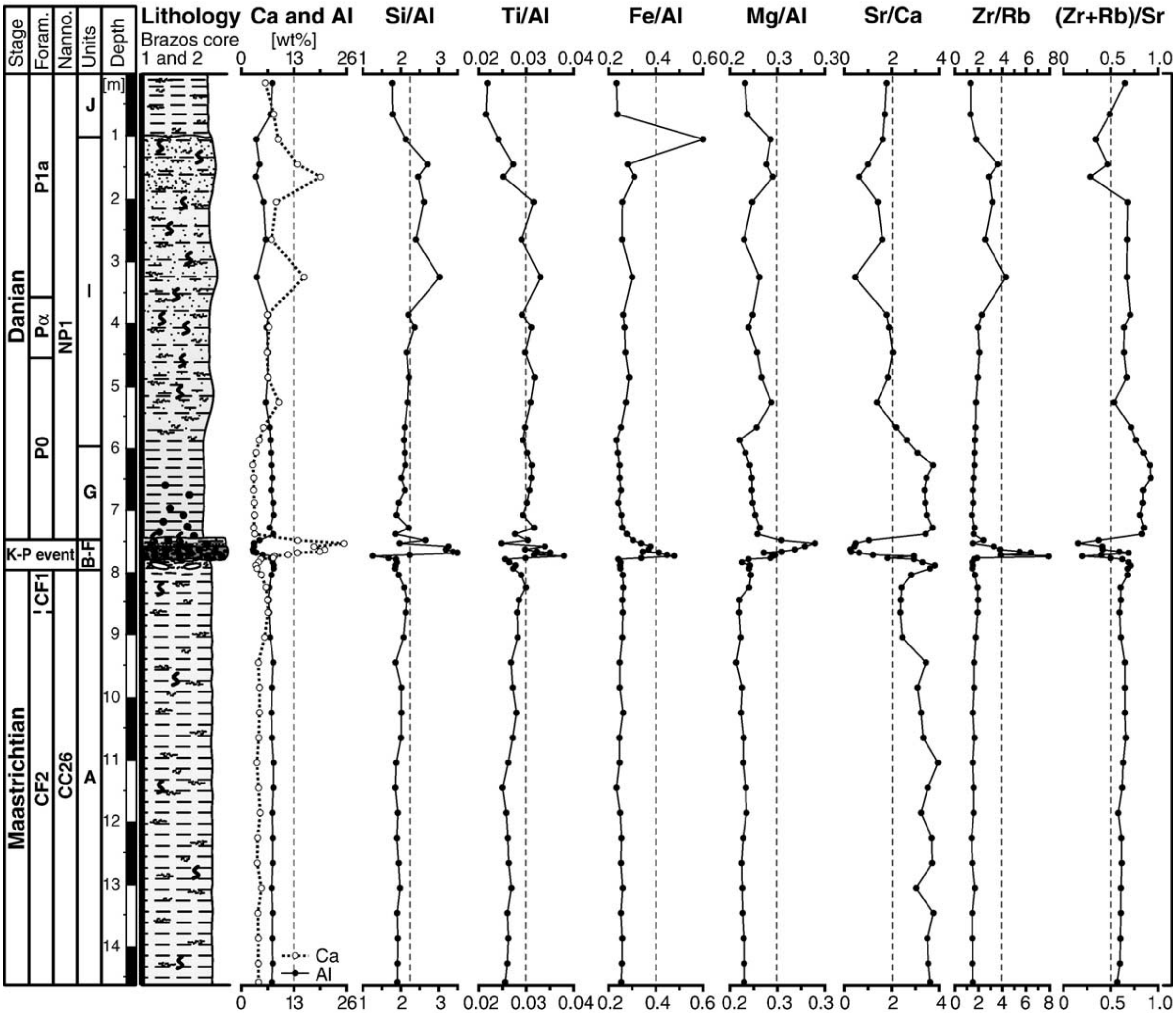

Fig. 7. Composite figure of the two Brazos cores showing the CaO contents and selected major and trace element ratios determined by WDS and EDS. For the element ratios, the major elements are given as mol, whereas the trace elements (Sr, Zr, Rb) are given as mmol. All Fe are given as Fe_2O_3. A legend is provided in Fig. 3.

suggesting an increase in fine-grained terrigeneous detritus, probably derived from clay minerals or feldspars.

3.5. Magnetic susceptibility

Rock magnetic parameters such as magnetic susceptibility (MS) provide information on the concentration of ferrimagnetic, mainly iron oxides and iron sulfides, and paramagnetic minerals (e.g., Butler, 1998). Magnetic particles can sensitively reflect climatically or sea level modulated changes in the depositional realm, because mineralogy, concentration and grain size of iron minerals are related to environmental conditions (Dekkers, 1997; Maher et al., 1999; Köβler et al., 2001). Specifically, the magnetic susceptibility is interesting in a climatic context because it has been used successfully as climatic proxy in several studies (e.g., Robinson, 1993; Arai et al., 1997; Barthés et al., 1999; Mayer and Appel, 1999; MacLeod et al., 2001). These studies have demonstrated pronounced climate dependence and coincidence with the Earth-orbital parameters driven by eolian dust load, dilution of magnetic detritus by biogenetic carbonate/silicate accumulation, or cyclic sedimentation resulting from climate-related changes in continental runoff.

The MS signature of the Brazos K–P boundary sections (Fig. 8) exhibits quite constant low paramagnetic susceptibility values ($<100\times10^{-6}$ Si/g) for the latest Maastrichtian Corsicana shales with a weak low-

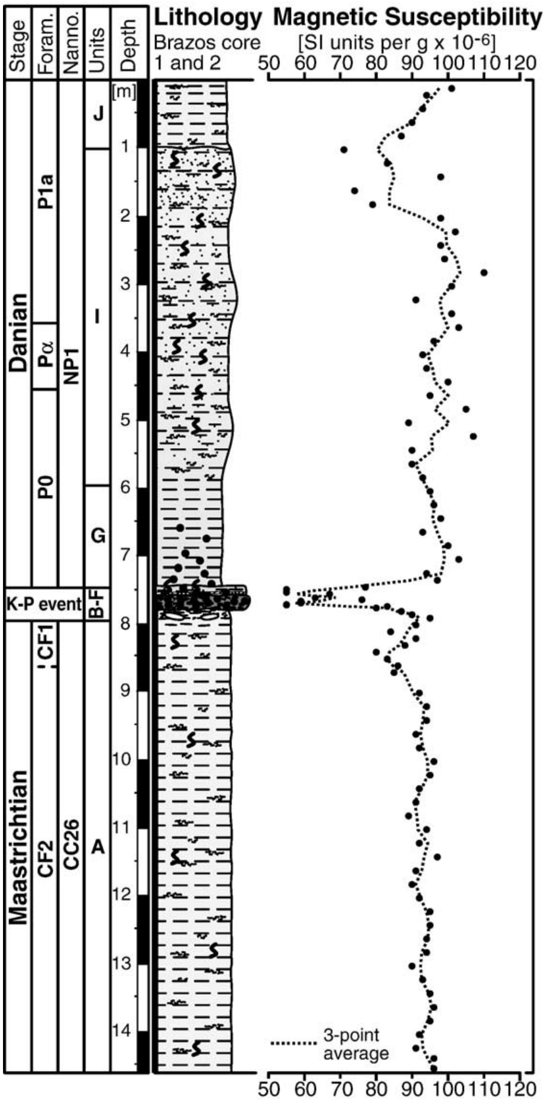

Fig. 8. Composite figure of the two Brazos cores with the magnetic susceptibility (MS). A legend is provided in Fig. 3.

amplitude cyclic (or rhythmic) pattern. The wavelength of the cycles is between 1 and 1.5 m. In the meter immediate below the event deposit, a slight lowering of the MS occurs which parallels the increase in (diamagnetic) carbonate content and in foraminiferal abundance. The K–P event deposit is characterized by an abrupt decrease of the MS ($<60\times10^{-6}$ Si/g), which is related to the deposition of smectite- and (diamagnetic) carbonate-rich ejecta. Low, paramagnetic MS values are characteristic for proximal K–P sites, resulting from the high amount of target rock material in the ejecta (e.g., Sigurdsson et al., 1997; Schulte and Kontny, 2005), whereas distal K–P sites generally reveal a high, ferromagnetic MS values, reflecting the input of mainly bolide material (e.g., Worm and Banerjee, 1987; Kletetschka et al., 2001; Ellwood et al., 2003). Immediately above the event deposit, the magnetic susceptibility increases again to pre-event values at the base of the Unit G shales. Within the carbonate-poor Unit G, the MS values then decrease gradually up to the base of the carbonate-rich Unit I. This decline may be related to the gradual increase of productivity during deposition of Unit G following the K–P event. Further up-section, the MS of Units I and J shows scattered values that are superimposed on a broad cyclic pattern with a wavelength of about 1.5 m, although no clear correlation between the MS and Ca content is apparent (as also revealed by plotting the MS vs. the Ca content of the samples resulting in $r^2=0.47$). The MS declines during the bioturbated uppermost part of Unit I, probably due to the increase in coarse silicic detritus.

3.6. Petrography and mineralogy of the event deposit

Microphotographs of the spherule-rich basal part (Unit C) of the K–P event deposit show a chaotic, microbreccia-like texture with rare preferred orientation of grains (Fig. 9A, B). No apparent cementation has been observed and the components are 'loosely' floating in a micritic matrix. The component shapes range from rounded particles to elongated–irregular fragments without any distinct abrasion-textures; grain sizes vary in a broad range from about 0.1 to 2 mm in diameter. The following components were encountered in the spherule-rich basal part of the K–P event deposit by thin-section analysis and backscattered EMP imaging (see Figs. 9 and 10) and are listed in order of decreasing abundance:

- Rounded to irregular flaser-like schlieren-rich ejecta spherules of brown to green color (Fig. 9A–C). They are either opaque or green–brown color in plain light, in part with high birefringence under crossed nicols. They have similar shapes and forms to other K–P spherules found in Mexico and Alabama (Schulte, 2003). The spherules are frequently fringed by calcite with outward radiating crystals and/or pseudomorphical replacement by numerous tiny pyrite crystals. Some may have been flattened by compaction. Spherules show internal structures, including vesicles, flow-patterns, and dark lamellae. Further mineralogical characterization of the ejecta spherules is done by electron microprobe analysis as outlined below.

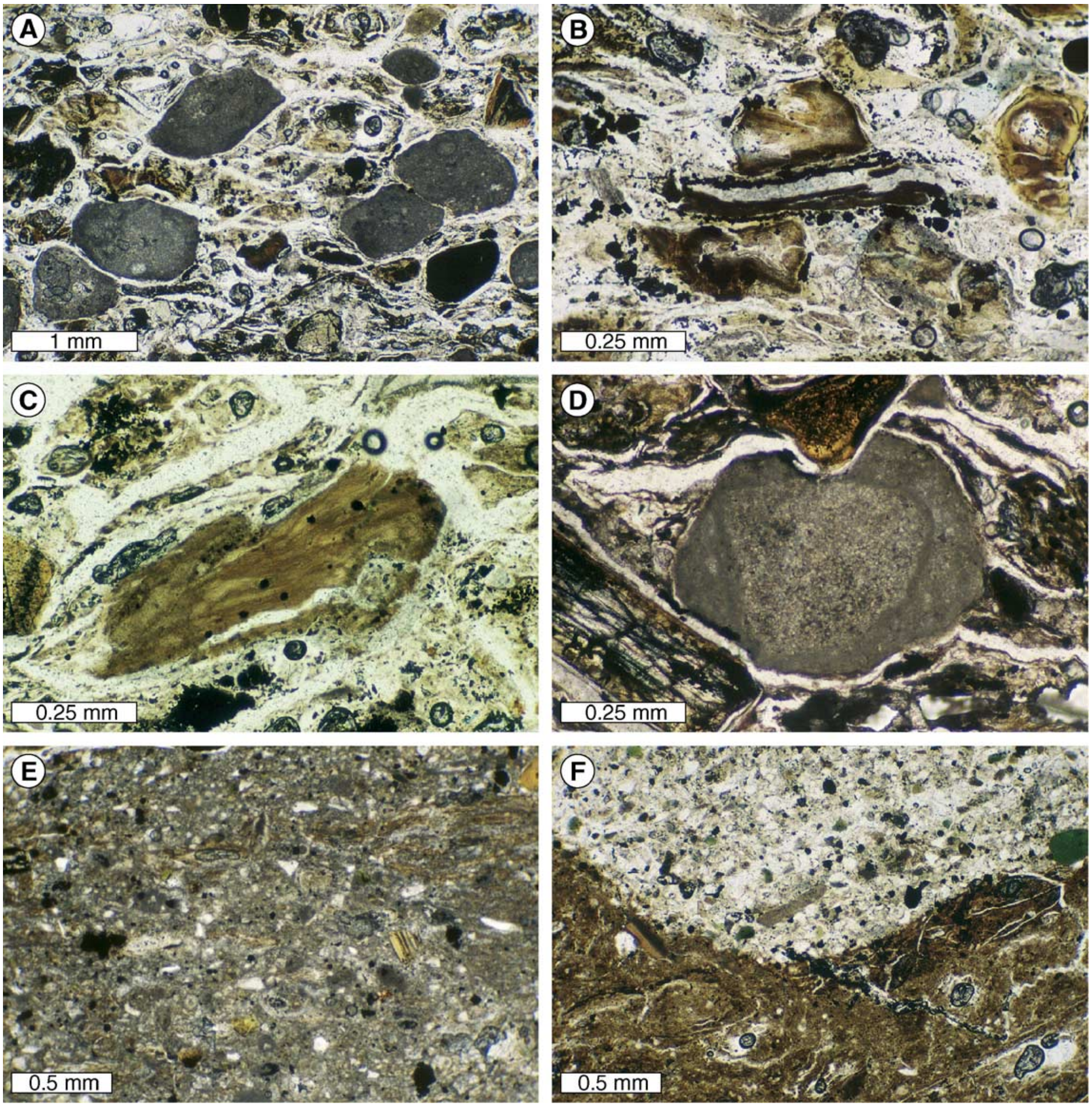

Fig. 9. Thin section photos of lithologies from the event deposit in the Brazos cores showing characteristic features of microfacies and components in plane-polarized light. (A) Microbreccia-like unit C with spherules, opaque phases, limestone clasts, accretionary lapilli, phosphatized particles, and fossil debris (unit C, sample BZC2-43). Note near-absence of quartz or feldspar. (B) Brown spherules and fragments (unit C, BZC2-43). Spherules are hollow and show thin lamellae of Ti–Fe-rich oxides. (C) Irregular smectitic fragment with opaque inclusions (unit C, BZC2-42). Note schlieren with flow-structures and opaque inclusions. (D) Lithoclast with internal concentric structure interpreted as accretionary lapilli (unit C, BZC2-42). (E) Carbonate-rich 'sandstone' from unit D–E (BZC2-46). Components include limestone grains, smectitic grains, opaque phases, phosphatized detritus, and foraminifera. Note rare presence of quartz or feldspar grains. (F) Silty layer incised in the upper fine-grained part of the micritic limestone from unit D–E (BZC1-10). The well-sorted siltstone contains opaque phases, phosphatized detritus, and fossil fragments as accessory components.

- Carbonate fluorapatite (CFA), including rounded to irregular shaped grains, mollusk shell debris, fish teeth, and bone fragments (Fig. 9A).
- Tiny mm-sized limestone clasts with 'lapilli-like' accretionary features (Fig. 9D).

In addition, benthic foraminifera, glauconite, abundant pyrite, iron oxides and -hydroxides (hematite, goethite), rare plant remains, as well as fine sand- to silt-sized quartz grains are present in the basal part of the K–P event deposit. Among these constituents, pyrite is quite prominent, since it occurs not only as dispersed euhedral crystals, but it also pseudomorphologically replaces spherules (Fig. 10A) and constitutes pyrite framboids of 20–50 μm in diameter (Fig. 10B).

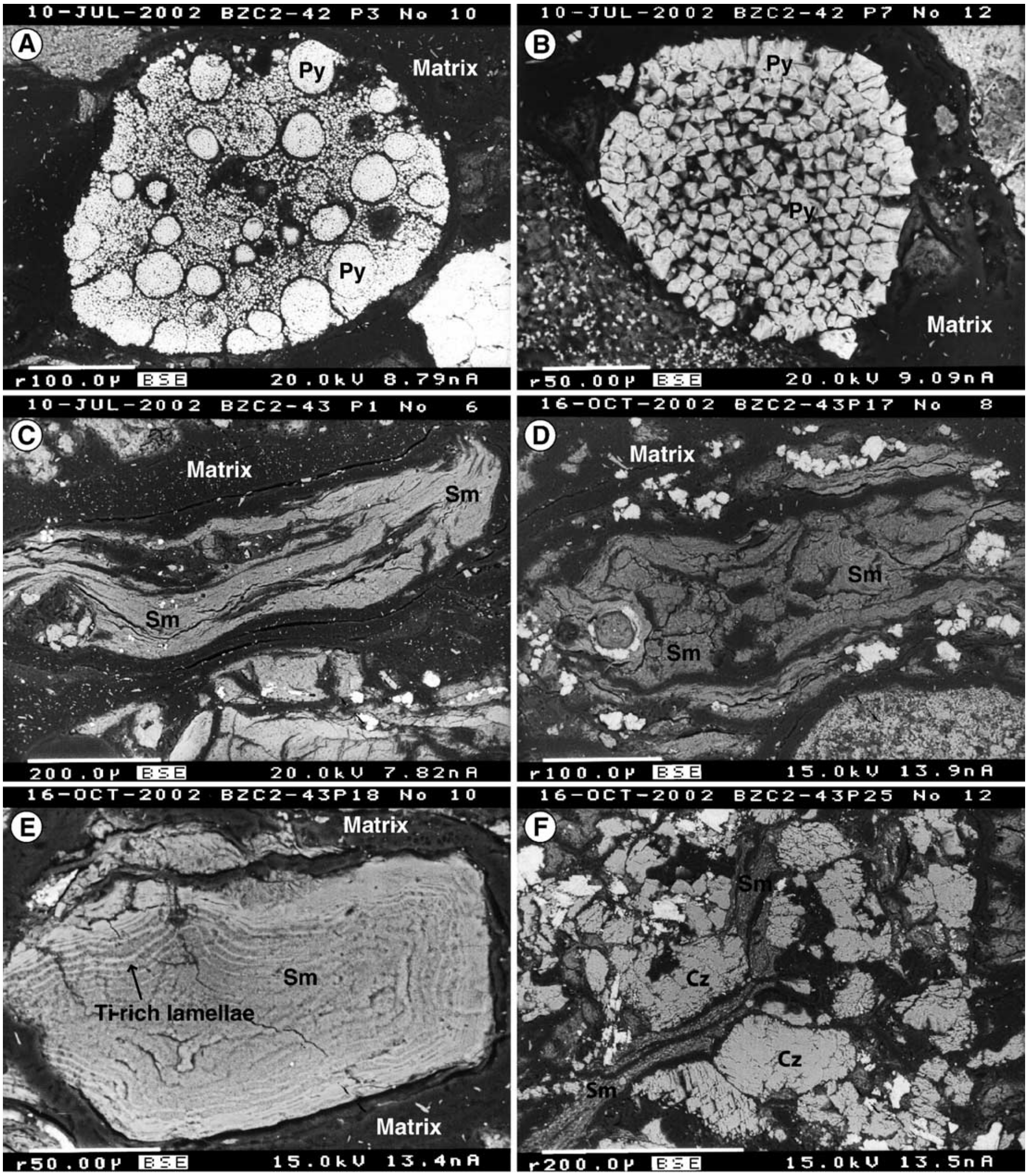

Fig. 10. Backscattered electron (BSE) images of components from the spherule-rich deposit at the base of the event deposit in the Brazos cores (unit C). Dark matrix is resin from embedding. Abbreviations: Sm = smectite; Py = pyrite; Cc = calcite. (A) Spherule, which is pseudomorphically replaced by tiny pyrite crystals. (B) Framboidal pyrite. (C and D) Flaser-like smectite and chlorite ejecta fragments. Note flow-structure and delicate outlines as well as abundance of bright (opaque) phases, including predominantly pyrite and hematite. (E) Details of smectite ejecta clasts with Ti-rich lamellae. (F) Flaser-like clayey ejecta fragments enveloping carbonate fragments and vice versa. Note similarity to textures from spherule deposits in northeastern Mexico (Schulte and Kontny, 2005).

We applied wavelength-dispersive electron microprobe (EMP) analysis to investigate the mineralogical composition of the ejecta spherules. Some 4–10 points were analyzed on each individual ejecta spherule to assure reliable average values and a reasonable measure of compositional variability. The stoichiometric conversion of oxide-weight percentage into formula units yields reasonable cation sums for both smectites and chlorites, indicating that the mineral analyses are affirmative. The results of the EMP analysis show low oxide totals between 70 and 90 wt.%. This implies copious amounts of low-Z materials, commonly H_2O or CO_2 that are typical for clay minerals (e.g., smectite; Newman and Brown, 1987). The geochemical compo-

Table 2
Chemical composition and calculated structural formulae of representative smectite and chlorite spherules from unit C of the Brazos core 2

Sample	Smectite									Chlorite			
	2–43	2–43	2–42	2–43	2–43	2–43	2–43	2–43	2–42	2–43	2–43	2–43	2–43
Number	P3 (wt.%)	P2 (wt.%)	P9 (wt.%)	P4 (wt.%)	P30 (wt.%)	P28 (wt.%)	P16 (wt.%)	P35 (wt.%)	P5 (wt.%)	P19 (wt.%)	P9 (wt.%)	P8 (wt.%)	P22 (wt.%)
SiO_2	59.29	59.46	60.83	59.03	57.58	55.81	55.79	57.53	53.87	33.56	30.69	31.13	30.36
TiO_2	0.19	0.19	0.15	0.16	0.37	0.39	1.26	0.99	0.06	0.61	0.31	0.21	2.00
Al_2O_3	23.31	22.21	24.40	23.87	23.29	23.67	24.15	23.57	22.87	18.22	16.90	17.09	15.94
FeO	0.71	0.70	0.70	0.76	0.70	0.63	0.74	0.70	4.07	18.77	21.19	21.69	21.64
MgO	3.90	4.16	4.03	3.75	3.91	3.67	2.76	3.55	4.56	7.05	8.05	10.51	9.03
CaO	0.03	0.06	0.04	0.04	0.07	0.05	0.07	0.05	0.10	0.13	0.16	0.15	0.27
Na_2O	0.08	0.04	0.05	0.01	0.05	0.09	0.08	0.08	0.09	0.09	0.11	0.13	0.09
K_2O	1.25	1.15	1.23	1.14	1.12	1.12	1.19	1.17	0.90	0.23	0.28	0.27	0.14
Total	88.80	88.11	91.44	88.82	87.11	85.46	86.11	87.69	86.56	78.80	77.73	81.21	79.54
	Numbers of cations per half structural unit cell												
Si	3.88	3.93	3.87	3.87	3.85	3.80	3.78	3.82	3.71	3.70	3.52	3.43	3.43
Al(IV)	0.12	0.07	0.13	0.13	0.15	0.20	0.22	0.18	0.29	0.30	0.48	0.57	0.57
Σ(Tetra)	4.00	4.00	4.00	4.00	4.00	4.00	4.00	4.00	4.00	4.00	4.00	4.00	4.00
Al(VI)	1.68	1.66	1.70	1.71	1.68	1.71	1.71	1.67	1.57	2.07	1.81	1.65	1.56
Fe	0.04	0.04	0.04	0.04	0.04	0.04	0.04	0.04	0.23	1.73	2.03	2.00	2.05
Mg	0.38	0.41	0.38	0.37	0.39	0.37	0.28	0.35	0.47	1.16	1.38	1.73	1.52
Ti	0.02	0.02	0.01	0.02	0.04	0.04	0.13	0.10	0.01	0.10	0.05	0.03	0.34
Σ(Octa)	2.12	2.12	2.13	2.13	2.15	2.16	2.16	2.16	2.28	5.07	5.28	5.41	5.46
Ca	0.00	0.00	0.00	0.00	0.00	0.00	0.00	0.00	0.00	0.01	0.01	0.01	0.02
Na	0.01	0.00	0.00	0.00	0.00	0.01	0.01	0.01	0.01	0.01	0.01	0.01	0.01
K	0.09	0.08	0.08	0.08	0.08	0.08	0.09	0.08	0.07	0.03	0.03	0.03	0.02
Σ(Inter)	0.09	0.09	0.09	0.08	0.09	0.09	0.09	0.09	0.08	0.04	0.06	0.05	0.04
Fe/(Fe+Mg)	0.09	0.09	0.09	0.10	0.09	0.09	0.13	0.10	0.33	0.60	0.60	0.54	0.57

Smectite analyses were calculated on basis of $O_{10}(OH)_2$, chlorite analyses on the basis of $O_{10}(OH)_8$. Tetra = tetrahedral; Octa = octahedral; Inter = interlayered.

Table 3
Calculated structural formulae of representative smectite analysis (on the basis of $O_{10}(OH)_2$) from the spherule deposits in the Brazos core 2 compared to smectite analysis from K–P boundary spherules and K–P clay layers

Locality	Brazos	Brazos	Beloc	Beloc	ODP 1049A	DSDP 390B	Stevens Klint	Agost
Region	Texas	Texas	Haiti	Haiti	W-Atlantic	W-Atlantic	Denmark	Spain
Material	Spherule	Spherule	Spherule	Spherule	Spherules	Spherule	K–P Clay	K–P Clay
References	This study	This study	Koeberl and Sigurdsson (1992)	Bauluz et al. (2000)	Martínez-Ruiz et al. (2001c)	Klaver et al. (1987)	Ortega-Huertas et al. (1998)	
	Numbers of cations per half structural unit cell							
Si	3.93	3.71	4.00	3.91	3.66	3.74	3.96	3.60
Al(IV)	0.07	0.29	0.00	0.09	0.34	0.26	0.04	0.40
Σ(Tetra)	4.00	4.00	4.00	4.00	4.00	4.00	4.00	4.00
Al(VI)	1.66	1.57	1.17	1.04	1.84	1.26	1.29	1.40
Fe	0.04	0.23	0.37	0.44	0.71	0.63	0.24	0.48
Mg	0.41	0.47	0.68	0.62	0.48	0.27	0.69	0.20
Ti	0.02	0.01	0.06	0.01	0.03	0.05	0.01	0.01
Σ(Octa)	2.12	2.28	2.29	2.11	3.06	2.22	2.23	2.09
Ca	0.00	0.00	0.12	0.36	0.02	0.01	0.15	0.02
Na	0.00	0.01	0.00	0.01	0.01	0.07	0.00	0.01
K	0.08	0.07	0.01	0.13	0.22	0.21	0.00	0.39
Σ(Inter)	0.09	0.08	0.13	0.50	0.25	0.29	0.15	0.42
Fe/(Fe+Mg)	0.09	0.33	0.35	0.42	0.60	0.70	0.26	0.71

Tetra = tetrahedral; Octa = octahedral; Inter = interlayered.

Table 4
Calculated structural formulae of representative chlorite analysis (on the basis of $O_{10}(OH)_8$) from the event deposit in Brazos core 2 and from spherule deposits in northeastern Mexico (Schulte and Kontny, 2005)

Locality	Brazos	Brazos	La Sierrita	El Mimbral
Region	Texas	Texas	NE Mexico	NE Mexico
Material	Spherule	Spherule	Spherule	Spherule
References	This study	This study	Schulte and Kontny (2005)	
	Numbers of cations per half structural unit cell			
Si	3.43	3.43	3.06	3.40
Al(IV)	0.57	0.57	0.94	0.60
Σ(Tetra)	4.00	4.00	4.00	4.00
Al(VI)	1.65	1.56	1.78	1.51
Fe	2.00	2.05	2.07	1.67
Mg	1.73	1.52	1.65	2.27
Ti	0.03	0.34	0.01	0.00
Σ(Octa)	5.41	5.46	5.51	5.45
Ca	0.01	0.02	0.03	0.06
Na	0.01	0.01	0.01	0.01
K	0.03	0.02	0.04	0.02
Σ(Inter)	0.05	0.04	0.07	0.09
Fe/(Fe+Mg)	0.54	0.57	0.56	0.42

Tetra = tetrahedral; Octa = octahedral; Inter = interlayered.

sition of the spherules is shown in Table 2; a comparison with smectite and chlorite spherules from other K–P sections is provided in Tables 3 and 4.

Smectite spherules have high SiO_2 (54–60 wt.%), Al_2O_3 (22–24 wt.%), MgO (3–5 wt.%), and show minor values for K_2O (~1 wt.%), FeO (<1 wt.%), whereas Na_2O, TiO_2, and CaO are generally well below 0.5 wt.%. In addition, the smectite spherules contain iron-hydroxides (e.g., hematite crystals), pyrite crystals, and schlieren of TiO_2 (up to 10 wt.%) and FeO (up to 7 wt.%). In addition, schlieren and inclusions of low SiO_2 (30 wt.%), high FeO (20 wt.%), and high MgO (10 wt.%) are present. Their totals are between 80 and 90 wt.%. This geochemical composition is equivalent to Mg-enriched dioctahedral smectite as shown by the characteristic cation sums when normalized to $O_{10}(OH)_2$ (Newman and Brown, 1987). The $(Al+Fe)^{VI}/Mg^{VI}$ ratio of 1.7/0.4, which is typical for smectites, substantiates this classification (Grauby et al., 1993). Following the geochemical criteria provided by Güven (1988), these smectites belong to the beidellite–nontronite series. However, sums for the cations occupying the octahedral sites exceed the ideal value of two by 0.1–0.3 and indicate a slight trioctahedral character of the smectite (Newman and Brown, 1987).

Chlorite spherules have high amounts of FeO (18–22 wt.%) and MgO (7–11 wt.%) and considerable lower SiO_2 (30–34 wt.%) and Al_2O_3 (16–18 wt.%) contents compared to the smectite spherules outlined above. The oxides K_2O, Na_2O, TiO_2, and CaO are generally between 0.5 wt.% and their totals sum up to 78–82 wt.%. Normalization to $O_{10}(OH)_8$, showed cation sums indicative for chlorite (Newman and Brown, 1987; Bailey, 1988). The number of octahedral cations per formula unit is between 5 and 6, with mean values of about 5.4. This composition corresponds to an intermediate composition between di,trioctahedral chlorites (5 cations) and trioctahedral chlorites (5.5–6.1 cations, see Newman and Brown, 1987). The predominance of Fe in the octahedral layer points to a chamosite-like composition. However, the high silica content (Si > 3–3.4 per formula unit), an Al^{VI} (1.5–2) contents much larger than the Al^{IV} (0.3–0.6) content, and a total octahedral occupation lower than 6 cations, suggests that some interlayers (e.g., smectite) are present (Shau et al., 1991).

4. Interpretation and discussion

4.1. Stratigraphy and placement of the K–P boundary

Before discussing the environmental changes across the K–P boundary, it is essential to evaluate (i) the Maastrichtian stratigraphic record, (ii) the placement of the K–P boundary, and (iii) the stratigraphic record of the early Danian.

4.1.1. (i) The Maastrichtian stratigraphic record

The composition of the late Maastrichtian calcareous nannofossil and planktic foraminifera assemblages indicates stable environmental conditions up to the event deposit. There is no evidence for significant hiatuses from the sedimentological, mineralogical and paleontological record. On the other hand, the respective index fossils for the latest Maastrichtian biozones are missing (CC26b, *M. prinsii*) or very rare (CF1, *P. reicheli*), although the nannofossil investigations of Mai et al. (2003) of the Brazos cores and of Jiang and Gartner (1986) suggest that the uppermost Maastrichtian is almost complete at the Brazos area. Previous outcrop studies of the Brazos area have revealed that the relief induced by erosion may reach up to no more than 0.2 to 0.7 m (Hansen et al., 1987, 1993b; Yancey, 1996). This would indicate maximum erosion of late Maastrichtian shales in the range of 40 to 120 ka based on a sedimentation rate of about 0.4–0.5 cm/ka given by Hansen et al. (1993b). In conclusion, it is difficult to establish the amount of erosion of the late

Maastrichtian shale and the associated duration of the hiatus that is associated with the unconformity at the base of the K–P event deposit.

4.1.2. (ii) Placement of the K–P boundary

The base of the boundary clay at El Kef, Tunisia, has been defined to mark the position of the global stratotype section and point (GSSP) for the Cretaceous–Paleogene boundary (Cowie et al., 1989). The basal, mm-thick K–P boundary clay layer contains peak iridium and siderophile–element concentrations, Ni-rich spinels, and goethite and smectite microspherules, interpreted as ejecta from the Chicxulub impact. The K–P boundary clay is also associated with a sudden drop in number and species (mass extinction and mass mortality) of Cretaceous calcareous nannofossils and (tropical) foraminifera (see summary in Keller et al., 1995; Remane et al., 1999), whereas new Paleocene species usually have their first appearance well above this iridium-rich clay layer (Olsson and Liu, 1993). The breakdown of carbonate productivity due to the mass extinction and mass mortality led also to an abrupt drop of the carbonate content and of the $^{13/12}C$ isotope ratio (D'Hondt et al., 1998). The concentration of boundary markers within one distinct mm-thick layer reflects the large distance of the El Kef GSSP to the Chicxulub impact site in Southern Mexico. In more proximal settings, the thickness of the K–P boundary clay increases significantly. In the Western Atlantic, for instance, the boundary clay, which is overlain by an iridium-rich layer, is about 6–15 cm thick, reflecting the increased amount of ejecta spherules in this area. In K–P site close to Chicxulub, e.g., in the Gulf of Mexico, the stratigraphy of the K–P boundary becomes even more complex due to further increased amounts of ejecta (e.g., constituting up to 1-m-thick layers in NE Mexico) and the effects of tsunami erosion and sedimentary disturbances (e.g., slumping and sliding).

Therefore, it is not surprising that our petrological, mineralogical, and geochemical analysis of both Brazos cores – as well as previous Gulf of Mexico K–P studies–revealed no evidence for the presence of a distinct mm-thick clay layer comparable to the "K–P boundary clay" in the El Kef GSSP in Tunisia. Instead, the classical boundary-markers occur in the event deposit (e.g., spherules) as well as in the overlying strata (e.g., multiple Ir anomalies, see Heymann et al., 1998). An analogous dispersion of the K–P boundary markers is also observed in the NE Mexican K–P sections (e.g., Schulte and Kontny, 2005) and in the Yaxcopoil core from within the Chicxulub crater (Arz et al., 2004; Smit et al., 2004). In consequence, we consider the event deposit to mark the K–P boundary. This position is in line with several sections in the Atlantic, the Pacific, the Western Interior, and the Tethyan realm, which all show a smectite spherule-rich bed at the K–P boundary (see Fig. 12 and Izett, 1990; Montanari, 1991; Schmitz, 1992; Bohor and Glass, 1995; Martínez-Ruiz et al., 1997; Ortega-Huertas et al., 1998; 2002; Bauluz et al., 2000; 2004; Wdowiak et al., 2001). For these sections, the K–P boundary clay layer has been linked to the Chicxulub impact event by a multitude of mineralogical and geochemical criteria. In addition, U–Pb dating of single shocked zircons from the K–P boundary clay in the Western Interior and from the Haitian spherule deposits at Beloc, as well as from the suevite from the Chicxulub impact structure, revealed similar source ages. This U–Pb ages suggest that these zircons derived from a common basement with an age of about 418 ± 6 Ma and 540 ± 10 Ma (e.g., Krogh et al., 1993a; 1993b; Kamo and Krogh, 1995). Moreover, a drop in carbonate contents due to reduced productivity and a decline of the nannofossil and foraminiferal abundance are a characteristic feature of many K–P boundary sections for the earliest Danian (Zones NP1 and P0, P1a: Henriksson, 1996; Gartner, 1996; Speijer and Van der Zwaan, 1996; Gardin and Monechi, 1998; Gardin, 2002; Håkansson and Thomsen, 1999; Culver, 2003; Bown, 2005).

Alternatively, some authors have placed the K–P boundary at the first appearance of Paleocene microfossils, which is about 1.6–1.8 m above the top of the event deposit in the Brazos cores of this study (Fig. 5A) and about 15–20 cm according to previous studies in the Brazos area (e.g., Jiang and Gartner, 1986; Keller, 1989a; Keller and Stinnesbeck, 1996). However, in K–P boundary sections, the first appearance of Paleocene microfossils is usually several centi- to decimeters above the K–P boundary clay and hence, their FAD can therefore not be used as a valid K–P boundary criterion (see discussion in Odin, 1992; Olsson and Liu, 1993; Bown, 2005). At Brazos, the planktic foraminifera and the calcareous nannofossils both show a significant drop in species number and abundance in the interval immediately overlying the event deposit without evidence that Cretaceous foraminifera and nannoplankton had recovered or were thriving after the impact (see also Pospichal, 1996b). Thus, it is reasonable to suggest that the nannoplankton and foraminifera extinction event occurred some time during the deposition of the clastic unit, and hence in association with the Chicxulub impact event at the K–P boundary.

4.1.3. (iii) The early Danian stratigraphic record

The early Danian in the Brazos core 1 reveals a complete and expanded succession of microfossil biozones and distinct evolutionary trends: The Danian planktic foraminifera fauna (P0, Pα, and P1a) is characterized by the successive appearance of newly evolved species (e.g., *Parvularugoglobigerina eugubina*), whereas the calcareous nannofossil flora (NP1a) shows consecutive blooms of various nannofossil species that, generally, originated already during the late Maastrichtian (e.g., *Neobiscutum romeinii*, *N. parvulum*, and *Cruciplacolithus primus*). However, the biozone P0 is extremely thick (>1.6 m), when compared to their thickness in other K–P boundary sections (usually 5 to 50 cm). Even in other cores or outcrops from the Brazos area, biozone P0 is at most 15–25 cm thick (Olsson and Liu, 1993). At present, there is no obvious explanation why the biozone P0 is so expanded in the Brazos core 2 and the core may be disturbed (for which there is no evidence from the data). Likewise, it may even reflect accumulation in a shallow depression or enhanced sedimentation behind an obstacle on the seafloor from a suspended cloud of silt and clay that settled out during long periods of low-energy conditions to form those units. In fact, the presence of reworked spherules and the gradual trends seen in the mineralogical and geochemical records (Figs. 6 and 7) may support such a scenario, as also suggested by Smit et al. (1996) on the basis of granulometric data. The paleogeographic setting of the Brazos area inside the inlet of the shallow Western Interior Seaway (see Fig. 1 and Kennedy et al., 1998), which probably modulated impact-triggered tsunamis and specifically their backflows, may provide a reasonable explanation for such a prolonged interval of sediment input.

4.2. Facies changes and sequence stratigraphic setting

The lithological as well as the mineralogical and geochemical data provide no support for distinct facies changes in the Corsicana shales (Unit A) up to the event deposit in the Brazos cores. Compositional changes are not as obvious as, for instance, in the shallower settings at central Alabama (Baum and Vail, 1988; Schulte, 2003). No significant long-term compositional trends have been observed, as also supported by the stable microfossil fauna (see Fig. 5). Hence, there is no evidence for significant facies changes during the late Maastrichtian that may be related to sea level fluctuations. This interpretation is consistent with data from Jiang and Gartner (1986), Bourgeois et al. (1988), Hansen et al. (1987; 1993a), and Yancey (1996) for the Brazos area.

Minor compositional changes of the Corsicana shales, however, occur in the 1.5-m-thick interval immediate below the event deposit, where an elevated carbonate contents (increase from ~6 to 9 wt.%) coincides with an increase in the abundance of foraminifera, tentatively suggesting a slight increase in productivity. From the Brazos outcrop sections, it is known that this interval is also associated with an increase in epibenthic suspension feeding bivalves (e.g., oysters), as well as with a drop in the molluscan diversity (Hansen et al., 1993b). Its (paleoecological) significance is yet unclear, and a relationship to regional climate changes or even the latest Maastrichtian warming event, which occurred between 400 and 100 ka before the K–P boundary (e.g., Olsson et al., 2001), may exist, although a link is difficult to constrain with the Maastrichtian biostratigraphic data from the core. Notably, a similar, although more pronounced increase of the carbonate content, coupled with elevated amounts of planktic foraminifera, has also been observed immediately below the K–P boundary and the basal sandy beds of the Clayton Formation in the Antioch Church core, Alabama (Schulte, 2003).

The lowered carbonate content of the laminated shales of the Littig Member (Unit G) above the K–P event bed is best explained by the decrease of the biogenic carbonate productivity commonly observed at the K–P boundary (Keller and Lindinger, 1989; Zachos et al., 1989; D'Hondt et al., 1998; Stüben et al., 2002a), since this layer is essentially devoid of macrofossil remains and drastically impoverished in microfossils (Fig. 5). Mineralogical and geochemical proxies indicate no changes in detritus composition that could be attributed to significant proximal–distal trends of the coastline and hence, to sea-level fluctuations.

The upper part of the Littig Member (Unit I) starts with the almost simultaneous occurrence of Paleocene microfossils and distinct nannofossil blooms (Fig. 5A), as well as with the gradual return of many invertebrates, mainly mollusks (see Hansen et al., 1987, 1993b). This interval is also associated with a gradual but marked change in the benthic foraminifera fauna (Midway assemblage, see Fig. 3). The sand and glauconite contents (and mica, see Figs. 3, 6 and 7) increases markedly in the uppermost strongly bioturbated meter of Unit I, and quartz reaches peak values (Fig. 6), suggesting increased proximity to the shoreline or a sea level lowering (Schutter, 1998). However, sections from Alabama, including the Antioch Church core (Schulte, 2003), reveal no evidence for a distinct lowstand during

Zone NP1 (Baum and Vail, 1988; Donovan et al., 1988). In fact, several parasequences, each associated with a distinct flooding surface, are present in this Zone in Alabama and a maximum flooding surface constitutes the upper limit of Zone NP1.

The carbonate content of the Littig Mm. reaches amounts similar to those of the Corsicana Formation upon the entry of the Paleogene fauna and further rises throughout the Zones Pα and P1a with peak values of 30 wt.%. This rapid increase of the carbonate values – and hence the increased productivity – is in marked contrast to observations from other K–P boundary locations from the Tethyan realm, including El Kef, Tunisia, where the carbonate content usually remains low from Zone P0 through at least the lower part of Zone P1b (Keller and Lindinger, 1989; Zachos et al., 1989; D'Hondt et al., 1998; Stüben et al., 2002a). Nevertheless, in sections from the Atlantic and the western Tethys, including Caravaca, Spain, the return to pre-K–P carbonate contents and thus higher marine productivity is more rapid and occurs already within Zone P0 or at the base of Zone P1α (e.g., Martínez-Ruiz et al., 2001a).

The shales of the Pisgah Member (Unit J) are separated from the underlying Littig Member by a pyritized and bioturbated horizon. Their mineralogical and geochemical composition, with decreasing quartz and feldspar contents, increasing smectite, as well as lower Si, Ti, and Mg rations versus Al shows a drastic facies change, suggesting a sudden increase in the distance to the shoreline (Van Wagoner et al., 1990; Schutter, 1998). Therefore, the base of the Pisgah Member is interpreted as a flooding surface (Van Wagoner et al., 1990; Schutter, 1998), an interpretation which is in line with the elevated smectite contents that is often associated with marine flooding periods (Chamley, 1997; Adatte et al., 2002). The stratigraphic position of this pyritized horizon in the Brazos core 1 is in keeping with the position of the "rusty pyrite concretion horizon" (RPH) within Zone P1a in the Brazos outcrop area by Yancey (1996).

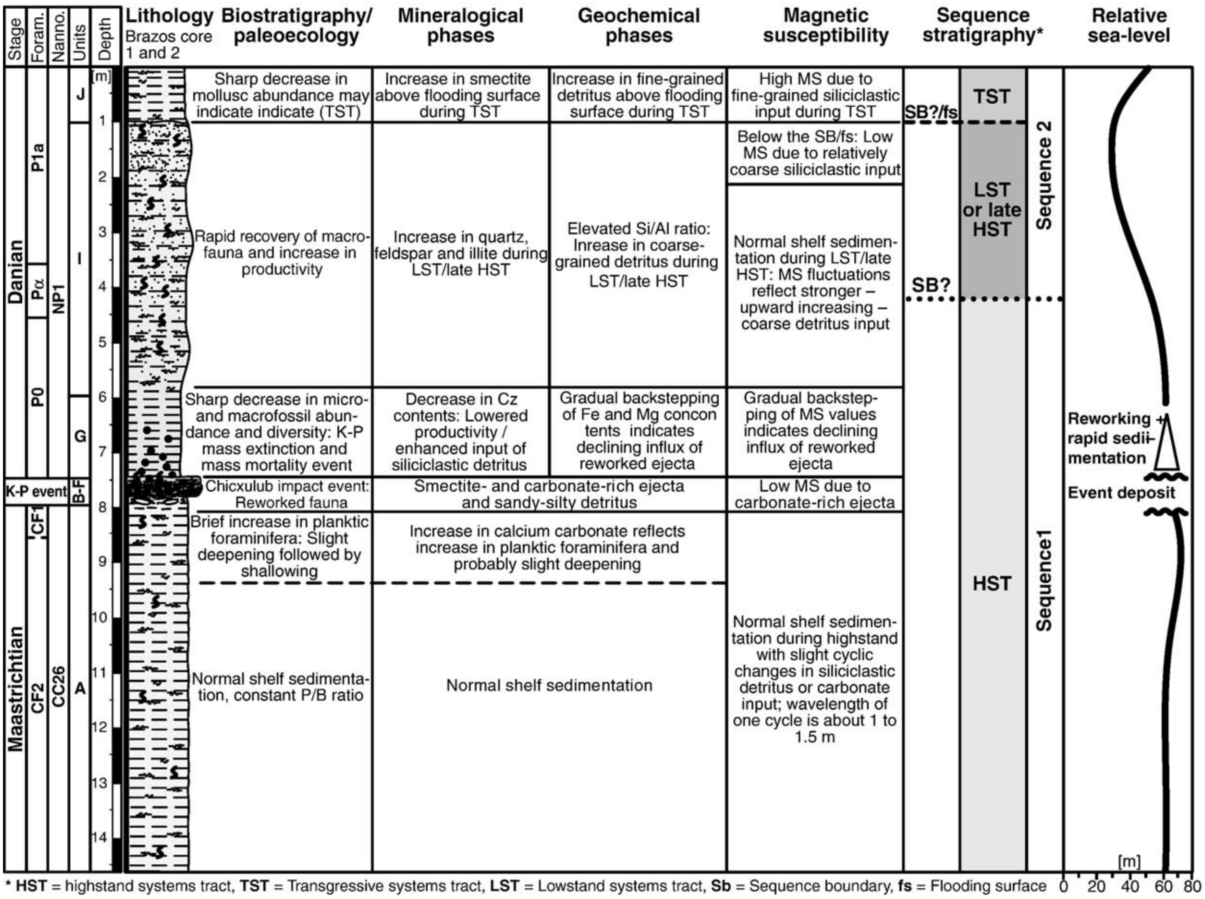

Fig. 11. Interpretation of ecological events and facies trends across the K–P boundary in the Brazos cores with suggested sequence stratigraphic setting and relative sea-level changes.

In conclusion, the following two scenarios are possible for the sequence stratigraphic setting of the K–P boundary in the Brazos area (Fig. 11):

(i) The Corsicana Fm. belongs to the highstand systems tract and the Littig Mm. of the Kincaid Fm. belongs to the late, regressive highstand systems tract, with shallowing and decreased proximity to the shoreline. The sequence boundary is thus situated at the transgressive pyritized horizon at the base of the Pisgah Mm.

(ii) Only the Corsicana Fm. belongs to the highstand systems tract and the Littig Mm. belongs to the lowstand systems tract. Hence, a type-2 sequence boundary would be situated in the upper part of the Littig Mm. and the base of the Pisgah Mm. would therefore be considered as a transgressive surface.

Further, more distinct interpretations can only be made by the detailed investigation of the K–P record in the Brazos region. However, both scenarios are in keeping with studies from adjacent areas that proposed a transgressive event at or immediately following the K–P boundary in the Dakotas (Johnson, 2002), in the Carolinas (Hargrove and Engelhardt, 1997), and in Alabama (e.g., Baum and Vail, 1988; Donovan et al., 1988; Schulte, 2003).

4.3. Cyclicity inferred from magnetic susceptibility

The shales of the Corsicana Fm. as well as the sandy–silty shales of the Littig Fm. show a rhythmic magnetic susceptibility pattern with wavelengths between 1 and 1.5 m. Such rhythmic sedimentation patterns are generally used to provide evidence for the presence of cyclic sedimentation, which can be ultimately linked to orbitally forced climate cycles (e.g., Schwarzacher, 2000). For instance, rhythmic bedding of Upper Cretaceous strata in the Western Interior has been successfully linked to eccentricity-driven climate changes (Ricken, 1994). However, in contrast to the Upper Cretaceous strata in the Western Interior, which show a carbonate vs. siliciclastic (c/s) ratio of 1:2, the Maastrichtian and Danian shales show a significant lower carbonate content (c/s ratios between 1:8 and 1:12, see Ricken, 1994). Consequently, the Corsicana and Littig shales should be by far less capable of transforming the (weak) climate cycles into rhythmic stratification. Comparing the magnetostratigraphically calibrated sedimentation rates (4.4 to 5.1 mm/ka for the latest Maastrichtian) given in Hansen et al. (1993b) or the duration of Zone CF1 (about 0.5 m equivalent to 300 ka) with the wavelength of one Brazos cycle (1 to 1.5 m) would correspond to about 230 to more than 600 ka for one cycle, which is out of tune with the known eccentricity periods of 100 and 400 ka. Therefore, it is not clear whether the very weak rhythmic MS patterns actually represent true rhythmic sedimentation resulting from Milankovitch cycles. Nevertheless, the amplitude of the earliest Danian sedimentary cycle increases significantly when compared the late Maastrichtian amplitudes (Fig. 8); a behavior that has been observed in a number of mid- to low-latitude K–P sections (see Dinarès-Turell et al., 2003; Hennebert and Dupuis, 2003). These authors explained the larger Danian cycle amplitudes by enhanced sensitivity to orbitally induced climate forcing following the K–P mass extinction.

4.4. Paleoclimate inferred from clay minerals

Considering the paleoclimate record inferred from clay mineral facies, we suggest that the relatively invariable smectite-dominated clay mineralogy of the shales in the Brazos cores documents detrital influx from soils that developed during chemical weathering in warm climates with wet and dry seasons (Chamley, 1997). On the other hand, smectite may be derived from the alteration of volcanic rocks or via burial diagenesis. However, taking into account an origin from volcanic sources, the continuous high abundance of smectite throughout the cores would require a permanent high volcanism in the Brazos area for which there is no evidence in this passive continental margin setting (Ewing and Caran, 1982). In addition, the sediments in the Texas coastal plain did not suffer deep burial diagenesis (Davidoff and Yancey, 1993). The absence of significant diagenetic overprint other than a transformation of impact glass into Mg-smectite and chlorite is documented by the constant presence of smectite, the near-absence of mixed-layers (e.g., illite–smectite), and the co-existence of smectite with kaolinite and chlorite. Moreover, in contrast to the well-crystallized smectite in the ejecta layer, the smectite in the shales of the Brazos cores is not well crystallized (see details in Schulte, 2003), probably Al-rich (beidelite), and supports a pedogenic, hence inherited origin.

Warm and humid to semiarid climate conditions were reported from paleosol studies from western Texas (Lehmann, 1990), as well as from Atlantic (Martínez-Ruiz et al., 2001b), and Tethyan (Chamley, 1997) domains throughout the K–P transition. These conditions favored the development of thick continental soils that led to the abundance of (Al-rich) smectites. In addition, smectites may have formed in poorly drained coastal areas resulting from tectonic stability, low continental relief, and warm, hydrolyzing climate conditions. According to the data reported here, these conditions may have prevailed in the Brazos hinterland during the latest Maastrichtian into the early Paleocene. The subordinate, albeit consistent amounts of illite, kaolinite, and chlorites, imply additional, simultaneous influx from (i) more mature (kaolinite) and (ii) from less evolved (illite, chlorite) types of soils (Blanc-Valleron and Thiry, 1997). Less evolved soils may have existed on uplifted regions, related to Laramide fold–thrust loading in northern Mexico and western Texas (Frank and Arthur, 1999).

4.5. Sedimentology of the K–P event deposit

The K–P event deposit in the Brazos cores records a complex sequence of sedimentary events: (i) strong currents associated with debris flows and soft-sediment disturbance (Unit B), (ii) deposition of locally reworked coarse ejecta that originally derived via air–water fallout to the seafloor (Unit C), followed by (iii) intermittent periods of sand–silt deposition (Unit D), (iv) deposition of finer-grained ejecta material (Units E and F), finally followed by (v) periods of reworking and settling (Unit G). This series of sedimentary events is analogous to other K–P sections in the Brazos area, although a distinct variability in thickness and extension of individual units exists (see Fig. 7 in Yancey, 1996). The 'ordered' succession of coarse ejecta particles overlain by finer-grained (sand- to silt-sized) ejecta suggests an upward decrease in the depositional energy. However, abrupt intermittent changes in the provenance of the sediments (ejecta material vs. terrigeneous detritus) make it very unlikely that the event deposit was deposited via a single instantaneous event (e.g., a single tsunami).

On the other hand, the presence of a cm-thick, graded ejecta sequence, as well as the absence of bioturbation in the units B, C and D, is difficult to explain by–more long-term–changes in the proximal–distal setting and/or sea-level fluctuations. Specifically, since there exists no evidence for abrupt facies changes from the mineralogical, geochemical, and paleontological data for the interval immediately above and below the event deposit (see previous Section 4.3). In consequence, an origin of the event deposit as incised valley fill during a pronounced sea-level lowstand and subsequent sea-level rise – as for instance proposed by Keller (1992) – is not supported by the sedimentological data.

We conclude that a series of depositional events, including tempestites and tsunamis, provides the best explanation for the sedimentary sequence recorded in the Brazos K–P event deposit. The record of multiple depositional events in the aftermath of the Chicxulub impact – acting over a distinct, yet brief period following the impact – is consistent with the sedimentological data from the Alabama shelf (e.g., Olsson et al., 1996), from northeastern Mexico (e.g., Smit et al., 1996; Schulte and Kontny, 2005), as well as from within the Chicxulub impact structure (e.g., Goto et al., 2004). Nevertheless, the high variability of storm- and tsunami-related event deposits makes it difficult to point out characteristics for either depositional mechanism. Moreover, the effects of a series of tsunami or storm events in the Western Interior Seaway are currently not known and probably difficult to model (see examples outlined in Scheffers and Kelletat, 2003). However, it is likely that the buffering effects of such an extensive shallow water mass may have modulated substantially the behavior of impact- or post-impact tsunami- and tempestite-generated currents.

4.6. Chicxulub ejecta

The sedimentology, petrology, mineralogy, and geochemistry of impact ejecta are generally used for constraining the location of the source crater, its geology, and the physical processes during the impact event (e.g., Montanari and Koeberl, 2000). In the Brazos cores, the thickness of the ejecta layer (about 10 cm) is well within the range observed at other K–P sections at Brazos (5 to 10 cm, see Yancey, 1996). This thickness fits quite reasonably to the clear trend of decreasing thickness of ejecta deposits from NE Mexico, (e.g., at El Mimbral about 0.5–1 m) to the Western Interior (in the Raton Basin about 1 cm). The decrease in transportation energy is also reflected in the decreasing ejecta grain-size with increasing distance from the Chicxulub structure: grain size of the spherules is largest at the El Mimbral locality (mm to cm-sized spherules) and smallest at Texas and Alabama mm-sized spherules), In comparison, at Blake Nose, western Atlantic, spherules are 1–2 mm in size, at Bass River, 0.2–1 mm, and in the Western Interior about 0.5–1 mm (see Fig. 1). In conclusion, the regional ejecta thickness distribution and grain-size pattern clearly suggests an origin for the ejecta spherules by the Chicxulub impact event, although reworking and redistribution of Chicxulub ejecta has likely occurred around the Gulf of Mexico.

A common origin by the Chicxulub impact is also reflected by the similar morphological characteristics of the ejecta spherules from the K–P boundary, including their rounded to irregular shapes and forms, as well as the presence of vesicles, schlieren, welding features, and accretionary spherules (e.g., Alvarez et al., 1992; Smit et al., 1996; Pope et al., 1999; Salge et al., 2000; Stüben et al., 2002b; Yancey, 2002; Schulte and Kontny, 2005). A comprehensive in-depth outline of the origination process of these ejecta particles is provided in numerous papers (e.g., Bohor and Glass, 1995; Smit, 1999; Claeys et al., 2002; Schulte and Kontny, 2005), and will not be repeated here. Consequently, only the most prominent features of the Brazos ejecta deposit will be discussed as well as analogies and differences to Chicxulub ejecta from K–P sections on a regional to global scale (Fig. 12).

Electron microprobe analysis revealed that most spherules from the Brazos K–P event bed are made of smectite with a distinct Mg-rich composition; in addition, some spherules have a chlorite-like mineralogy (Table 2). This composition suggests that the almost exclusive smectitic composition (>90% smectite from bulk rock analysis of the <2 μm fraction) of the ejecta layer (Unit C) is the result of an authigenic replacement of former glassy spherules. Mg- (and frequently Ca-) rich smectite is a common alteration product of Chicxulub ejecta spherules from K–P sections in the southern Gulf of Mexico, the Caribbean and the Western Atlantic (Ortega-Huertas et al., 1998; 2002; Debrabant et al., 1999). In addition, pronounced smectite enrichment has also been reported from a number of K–P sections in the eastern Atlantic, the Pacific, and the Tethyan realm to be associated with the basal (mm-thick) ejecta-fallout K–P clay layer and the alteration of microspherules (see review of Ortega-Huertas et al., 2002). The smectite composition from the Brazos spherules is well within the range given for these ejecta spherules (see comparison in Table 2 and Klaver et al., 1987; Bohor and Glass, 1995; Debrabant et al., 1999;

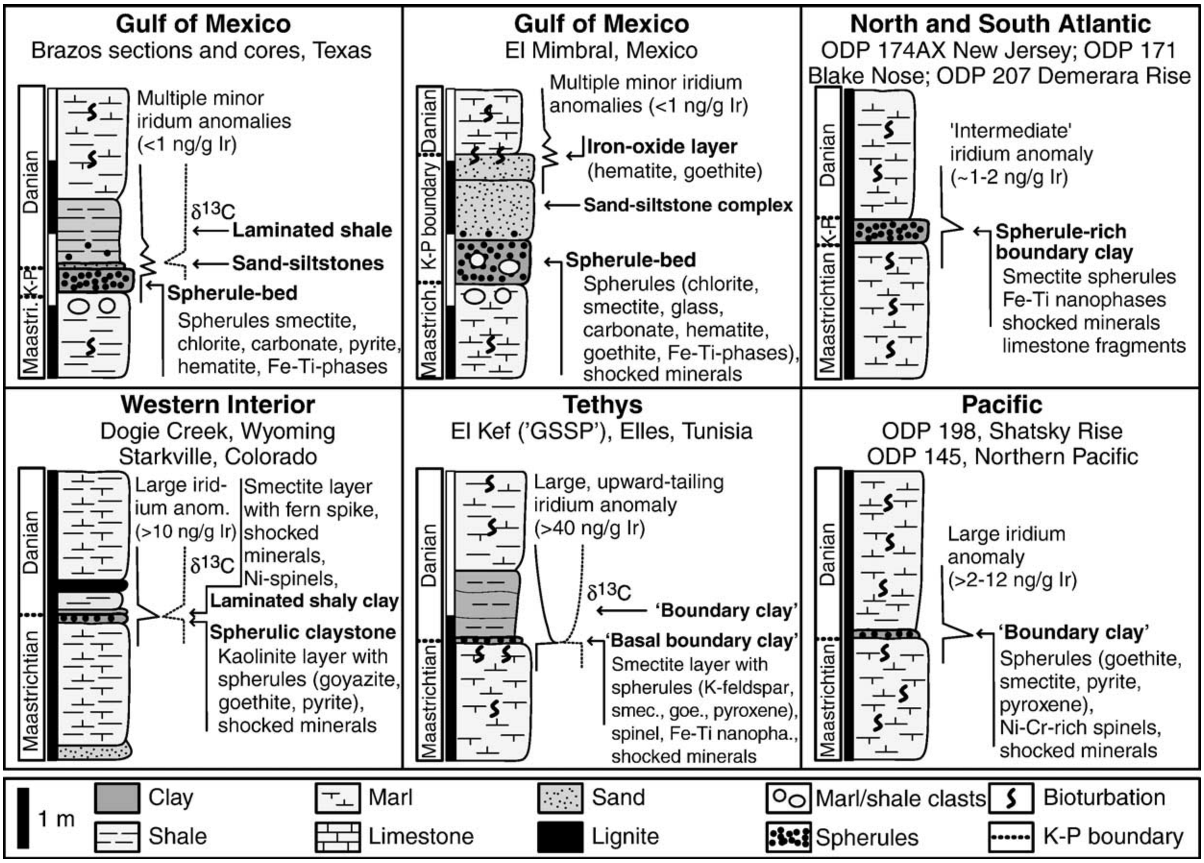

Fig. 12. Correlation of the K–P boundary in the Brazos core 2 to the K–P boundary in the Gulf of Mexico (Northeastern Mexico), the Western Interior (Raton Basin), the West Atlantic margin (ODP 171 and 174), the Tethyan realm (El Kef, GSSP stratotype section for the K–P boundary), and the Pacific Ocean (ODP 145 and 198). Note the "expanded" nature of the K–P boundary with intercalated siliciclastic (debris flow, tsunami or tempestite) deposits in the Gulf of Mexico.

Martínez-Ruiz et al., 2001c, 2002; Stüben et al., 2002a). These smectite spherules often contain glassy cores that by their geochemical composition point to a progenitor phase of andesitic composition, in line with the composition of melt fragments from Chicxulub impact structure (see Schuraytz et al., 1994; Kettrup et al., 2000; Kettrup and Deutsch, 2003; Claeys et al., 2003). Therefore, we suggest that the smectite spherules at Brazos derived via authigenesis from a similar parental phase of probably andesitic composition.

Spherules of chlorite mineralogy have rarely been observed from K–P spherule deposits in the Gulf of Mexico and adjacent areas, although they constitute the bulk of the ejecta particles in the spherule deposits of northeastern Mexico (see Schulte et al., 2003). The tabulated mineral compositions of typical chlorite from the Brazos core 2 and from northeastern Mexico in Table 4 show that the mineralogical composition of the Fe–Mg-rich di,trioctahedral, and trioctahedral chlorite ejecta particles are within the same range for both locations. For the ejecta from northeastern Mexico, a mafic precursor phase was suggested by previous studies (e.g., Schulte and Kontny, 2005), implying that mafic rocks may also account for the chlorite spherules in the Brazos area. Consequently, and in concert with the presence of Mg-rich smectite spherules, we suggest that the Brazos area in Texas received ejecta material from compositionally different (felsic vs. mafic) regions in the subsurface of the Chicxulub impact structure on the Yucatán peninsula, reflecting the petrological variability of the basement in the subsurface of the Chicxulub impact structure, as outlined by several previous studies (Kettrup et al., 2000; Kettrup and Deutsch, 2003), and specifically for the northwestern sector of the Chicxulub structure (Schulte and Kontny, 2005).

5. Conclusions

Based on the multidisciplinary evaluation of the K–P boundary interval in two cores from Brazos, Texas, we conclude the following.

5.1. Biostratigraphy, K–P faunal turnover and position of the K–P boundary

Foraminifera and nannofossil stratigraphy indicates that the Brazos cores include a latest Maastrichtian (Zone CF1–CF2 / CC26) and earliest Danian (P0, Pα and P1a/NP1) shale sequence with a sandy and Chicxulub ejecta-bearing event deposit at the K–P boundary; a hiatus of unknown duration may be present by the unconformable base of the event deposit. The Maastrichtian benthic foraminiferal fauna is stable, shows a sudden faunal change in the interval above the K–P event deposit, and a gradual change to a 'Midway' fauna within Zone Pα. Calcareous nannofossils show a rich flora in the latest Maastrichtian shales below the K–P event deposit, an impoverished flora above the event deposit, and an ordered succession of characteristic nannofossil bloom upon entry of the first Paleocene forms. However, during biozone P0 carbonate values reach and even exceed the carbonate contents of late Maastrichtian shales. This contrasts to other K–P boundary sections, for instance in the Tethyan realm, where the carbonate contents, and hence the productivity usually remains low up to Zone P1b, although K–P sections in the Atlantic and the Pacific usually show no lowered carbonate contents during these biozones.

The K–P event deposit is separated from the first occurrence of Paleocene microfossils by 1.6 m of laminated carbonate-poor shales that show an impoverished planktic foraminifera and nannofossil fauna, as well as almost no evidence for macrofauna remains, compared to the Maastrichtian shales below the event deposit. Trace element data provides no evidence for enhanced dys- or anoxic conditions for this interval. A similar interval is commonly present in the Brazos area, although with only about 15 to 25 cm thickness. Hence, the origin of this interval and possible reworking processes has to be evaluated within the local context of the Brazos outcrop area. However, in absence of characteristic K–P boundary clay, as revealed by the biostratigraphic, geochemical, and mineralogical data, we position the K–P boundary at the base of the event deposit, concomitant to the first appearance of Chicxulub ejecta. This position is in keeping with the occurrence of smectite-rich Chicxulub ejecta in the K–P boundary clay elsewhere (e.g., Atlantic, Pacific, Western Interior, Tethys). Consequently, our micropaleontological as well as our geochemical and mineralogical data provides no evidence that Chicxulub predated the K–P boundary, but instead strengthen the link between the Chicxulub impact and the K–P mass extinction.

5.2. Sequence stratigraphic setting and paleoclimate

No evidence for major proximal–distal facies trends is observed from the lithological, geochemical and mineralogical composition of the shales bracketing event deposit. The lowered carbonate content in the interval above the event deposit is attributed to the mass extinction resulting from the Chicxulub impact, possibly enhanced by dissolution. During the basal Danian Zone P0, multiple criteria (e.g., increased sand content) suggest regressive sea-level behavior (late highstand systems tract). The late highstand (or minor lowstand) systems tract is terminated at a pyritized horizon ("transgressive surface or type-2 sequence boundary") and overlain by the geochemically and mineralogically distinct transgressive systems tract.

The relatively constant clay mineral composition suggests that no major change occurred in the climate/weathering conditions across the K–P boundary at the Brazos region. The high smectite contents (>60%) flanked by minor illite, chlorite, and kaolinite points to warm, humid climates with pronounced seasonality, albeit the high diversity of this clay assemblage points to a complex hinterland with geologically and/or morphologically distinct compartments.

5.3. Sedimentology of the K–P event deposit

The complex, 20-cm-thick graded sedimentary sequence of the K–P event deposit in the Brazos cores is explained by ejecta deposition from debris flows and subsequent turbidite currents, with sudden intermittent provenance changes as indicated by thin intercalated pure quartzose sand–silt layers. This depositional sequence is probably resulting from successive tempestite or tsunami events. The top of this sequence is bioturbated and overlain by micritic limestone grading into laminated dark shales, suggesting deposition over a longer period. The basal part of the K–P event deposit contains clayey and vesiculated spherules generated by the Chicxulub impact, which in turn are observed at the K–P boundary in sections from other areas of the Gulf of Mexico, the Pacific, Northern America (Western Interior), and the western Atlantic.

5.4. Chicxulub ejecta

The ejecta particles are altered to clay minerals, including smectite and chlorite. In addition, tiny accretionary carbonate clasts are ubiquitously present in the basal part of the event deposit, which are interpreted to represent 'lapilli-like' ejecta derived from the accretion of fine carbonaceous dust. Smectite spherules are the main altered ejecta phase and their authigenesis led to the high amount of smectite in the basal units of the event deposit. These smectites are well crystallized, enriched in Mg, and compositionally belong to the beidellite–nontronite series. Mg-rich smectite derived from the alteration of microspherules is commonly observed in the basal K–P boundary clay layer in the Tethyan realm (Ortega-Huertas et al., 2002). The chlorites in the spherules are Fe–Mg-rich and have a chamosite-like composition, albeit with smectite interlayers. In summary, the wide compositional range of the ejecta spherules is interpreted as an inherited feature and suggests precursor glass phases of presumably mafic to intermediate character. This compositional spectrum is in line with the placement of the Brazos area between northeastern Mexico that received ejecta from mafic target rocks (now altered to chlorite), and the western Atlantic region, which received ejecta that derived from rocks of intermediate composition (now altered to Ca–Mg-rich smectite).

Acknowledgments

This study is part of the first author's PhD thesis and was supported by the German Science Foundation (DFG) via the International Continental Drilling Program (ICDP) (STI 128/7-1,2, STU 169/10-2 and KO 1514/1). The MS was written entirely by PS, with exception for the paragraph on benthic foraminifera, which was written by RS. RS provided the planktic and benthic foraminifera data and HM provided the calcareous nannofossil data. AK provided the magnetic susceptibility measurements. Sampling, sample preparation, evaluation, and interpretation of XRD, XRF and magnetic susceptibility data was conducted by PS, whereas Thierry Adatte (University of Neuchâtel) and Utz Kramar (Karlsruhe University) are both greatly acknowledged for providing the XRD and the XRF analysis. Wolfgang Stinnesbeck and Doris Stüben from the University of Karlsruhe are acknowledged for providing support and discussions. Gerta Keller, Princeton University, and Thor A. Hansen, Bellingham University, are thanked for comments and access to the Brazos cores from Texas. We are also indebted to Thomas E. Yancey, Texas A&M University, and two anonymous reviewers for constructive comments. Special thanks go to Volker Zibat from the Laboratory for Electron Microscopy and to Stefan Unrein from the sedimentary laboratory, both from the University Karlsruhe. In addition, we thank Armin Schafhauser (University Karlsruhe) for encouraging discussions and support.

References

Adatte, T., Keller, G., Stinnesbeck, W., 2002. Late Cretaceous to early Paleocene climate and sea-level fluctuations: the Tunisian record. Palaeogeography, Palaeoclimatology, Palaeoecology 178 (3–4), 165–196.

Alvarez, W., Smit, J., Lowrie, W., Asaro, F., Margolis, S.V., Claeys, P., Kastner, M., Hildebrand, A.R., 1992. Proximal impact deposits at the Cretaceous–Tertiary boundary in the Gulf of Mexico: a restudy of DSDP Leg 77, sites 536 and 540. Geology 20 (8), 697–700.

Arai, K., Sakai, H., Konishi, K., 1997. High-resolution rock-magnetic variability in shallow marine sediment: a sensitive paleoclimatic metronome. Sedimentary Geology 110 (1–2), 7–23.

Arz, J.A., Alegret, L., Arenillas, I., 2004. Foraminiferal biostratigraphy and environmental reconstruction at the Yaxcopoil-1 drillcore, Chicxulub crater, Yucatán Peninsula. Meteoritics and Planetary Science 39 (7), 1099–1111.

Bailey, S.W., 1988. Chlorites: structures and crystal chemistry. In: Bailey, S.W. (Ed.), Hydrous Phyllosilicates (Exclusive of Micas), Reviews in Mineralogy, vol. 19. Mineralogical Society of America, pp. 347–403.

Barthés, V., Pozzi, J.P., Vibert-Charbonnel, P., Thibal, J., Mélières, M.A., 1999. High-resolution chronostratigraphy from downhole susceptibility logging tuned by palaeoclimatic orbital frequencies. Earth and Planetary Science Letters 165 (1), 97–116.

Bauluz, B., Peacor, D.R., Elliott, W.C., 2000. Coexisting altered glass and Fe/Ni oxides at the Cretaceous/Tertiary boundary, Stevns Klint (Denmark): direct evidence of meteorite impact. Earth and Planetary Science Letters 182, 127–136.

Bauluz, B., Peacor, D.R., Hollis, C.J., 2004. TEM study of meteorite impact glass at New Zealand Cretaceous–Tertiary sites: evidence for multiple impacts or differentiation during global circulation? Earth and Planetary Science Letters 219 (3–4), 209–219.

Baum, G.R., Vail, P.R., 1988. Sequence stratigraphic concepts applied to Paleogene outcrops, Gulf and Atlantic basins. In: Wilgus, C.K., Hastings, B.S., Kendall, C.G., Posamentier, H.W., Ros, C., Van Wagoner, J.C. (Eds.), Sea-level Changes: An Integrated Approach, Special Publication, vol. 42. Society of Economic Paleontologists and Mineralogists, Tulsa, Oklahoma, pp. 309–327.

Bengtsson, H., Stevens, R.L., 1998. Source and grain-size influences upon the clay mineral distribution in the Skagerrak and northern Kattegat. Clay Minerals 33 (1), 3–13.

Berggren, W.A., Aubert, J., 1975. Paleocene benthonic foraminiferal biostratigraphy, paleobiogeography and paleoecology of Atlantic–Tethyan regions: midway-type fauna. Palaeogeography, Palaeoclimatology, Palaeoecology 18 (2), 73–192.

Berggren, W.A., Kent, D.V., Swisher, C.C., Aubry, M.-P., 1995. A revised Cenozoic geochronology and chronostratigraphy. In: Berggren, W.A., Kent, D.V., Aubry, M.-P., Hardenbol, J. (Eds.), Geochronology, Time Scales, and Global Stratigraphic Correlation, Special Publication, vol. 54. Society of Economic Paleontologists and Mineralogists, Tulsa, Oklahoma, pp. 129–212.

Biscaye, P.E., 1965. Mineralogy and sedimentation of recent deep-sea clay in the Atlantic Ocean and adjacent seas and oceans. Geological Society of America Bulletin 76 (7), 803–832.

Bitschene, P.R., Schmincke, H.-U., 1991. Fallout tephra layers: composition and significance. In: Heling, D., Rothe, P., Förstner, U., Stoffers, P. (Eds.), Sediments and Environmental Geochemistry. Springer, Heidelberg, Germany, pp. 48–82.

Blanc-Valleron, M.-M., Thiry, M., 1997. Clay minerals, paleoweathering, paleolandscapes and climatic sequences: the Paleogene continental deposits in France. In: Paquet, H., Clauer, N. (Eds.), Soils and Sediments: Mineralogy and Geochemistry. Springer, Heidelberg, Germany, pp. 223–247.

Bohor, B.F., Glass, B.P., 1995. Origin and diagenesis of K/T impact spherules—from Haiti to Wyoming and beyond. Meteoritics 30, 182–198.

Bourgeois, J., Hansen, T.A., Wiberg, P., Kauffman, E.G., 1988. A tsunami deposit at the Cretaceous–Tertiary boundary in Texas. Science 141, 567–570.

Bown, P., 2005. Selective calcareous nannoplankton survivorship at the Cretaceous–Tertiary boundary. Geology 33 (8), 653–656.

Bralower, T.J., Premoli-Silva, I., Malone, I., and Scientific Participants of ODP Leg 198, 2002. New evidence for abrupt climate change in the Cretaceous and Paleogene: an Ocean Drilling Program expedition to Shatsky Rise, northwest Pacific. GSA Today 12 (4), 4–10.

Brett, C.E., Allison, P.A., 1998. Paleontological approaches to the environmental interpretation of marine mudrocks. In: Schieber, J., Zimmerle, W., Sethi, P.S. (Eds.), Shales and Mudstones: I. Basin Studies, Sedimentology, and Paleontology. Schweizerbart, Stuttgart, Germany, pp. 301–349.

Butler, R.F., 1998. Paleomagnetism: Magnetic Domains to Geologic Terranes (electronic ed.). Department of Geosciences, Tucson, Arizona. 238 pp.

Cande, S.C., Kent, D.V., 1995. Revised calibration of the geomagnetic polarity timescale for the Late Cretaceous and Cenozoic. Journal of Geophysical Research 100 (B4), 6093–6095.

Chamley, H., 1997. Clay mineral sedimentation in the ocean. In: Paquet, H., Clauer, N. (Eds.), Soils and Sediments. Springer, Heidelberg, Germany, pp. 269–302.

Claeys, P., Kiessling, W., Alvarez, W., 2002. Distribution of Chicxulub ejecta at the Cretaceous–Tertiary boundary. In: Koeberl, C., MacLeod, K.G. (Eds.), Catastrophic Events and Mass Extinctions: Impacts and Beyond, Special Paper, vol. 356. Geological Society of America, Boulder, Colorado, pp. 55–68.

Claeys, P., Heuschkel, S., Lounejeva-Baturina, E., Sanchez-Rubio, G., Stöffler, D., 2003. The suevite of drill hole Yucatán 6 in the Chicxulub impact crater. Meteoritics and Planetary Science 38 (9), 1299–1317.

Cowie, J.W., Zieger, W., Remane, J., 1989. Stratigraphic commission accelerates progress, 1984–1989. Episodes 12 (2), 79–83.

Culver, S.J., 2003. Benthic foraminifera across the Cretaceous–Tertiary (K–T) boundary: a review. Marine Micropaleontology 47 (3–4), 177–226.

Davidoff, A.J., Yancey, T.E., 1993. Eustatic cyclicity in the Paleocene and Eocene: data from the Brazos River valley, Texas. Tectonophysics 222 (3–4), 371–395.

Debrabant, P., Fourcade, E., Chamley, H., Rocchia, R., Robin, E., Bellier, J.-P., Gardin, S., Thiébault, F., 1999. Les argiles de la transition Crétacé–Tertiaire au Guatemala, témoins d'un impact d'asteroide. Bulletin de la Société Géologique de France 170 (5), 643–660.

Deconinck, J.-F., Hesselbo, S.P., Debuisser, N., Averbuch, O., Baudin, F., Bessa, J., 2003. Environmental controls on clay mineralogy of an Early Jurassic mudrock (Blue Lias Formation, southern England). International Journal of Earth Sciences 92 (2), 255–266.

Dekkers, M.J., 1997. Environmental magnetism: an introduction. Geologie en Mijnbouw 76 (1–2), 163–182.

D'Hondt, S., Donaghay, P., Luttenberg, D., Lindinger, M., 1998. Organic carbon fluxes and ecological recovery from the Cretaceous–Tertiary mass extinction. Science 282, 276–278.

Dinarès-Turell, J., Baceta, J.I., Pujalte, V., Orue-Etxebarria, X., Bernaola, G., Lorito, S., 2003. Untangling the Palaeocene climatic rhythm: an astronomically calibrated Early Palaeocene magnetostratigraphy and biostratigraphy at Zumaia (Basque basin, northern Spain). Earth and Planetary Science Letters 216 (4), 501–514.

Donovan, A.D., Baum, G.R., Blechschmidt, G.L., Loutit, T.S., Pflum, C.E., Vail, P.R., 1988. Sequence stratigraphic setting of the Cretaceous–Tertiary boundary in central Alabama. In: Wilgus, C.K., Hastings, B.S., Kendall, C.G., Posamentier, H.W., Ros, C., Van Wagoner, J.C. (Eds.), Sea-level Changes: An Integrated Approach, Special Publication, vol. 42. Society of Economic Paleontologists and Mineralogists, Tulsa, Oklahoma, pp. 299–307.

Dypvik, H., Harris, N.B., 2001. Geochemical facies analysis of fine-grained siliciclastics using Th/U, Zr/Rb and (Zr+Rb)/Sr ratios. Chemical Geology 181 (1–4), 131–146.

Elderfield, H., Bertam, C.J., Erez, J., 1996. A biomineralization model for the incorporation of trace elements into foraminiferal calcium carbonate. Earth and Planetary Science Letters 142 (3–4), 409–423.

Ellwood, B.B., MacDonald, W.D., Wheeler, C.W., Benoist, S.L., 2003. The K–T boundary in Oman: identified using magnetic susceptibility field measurements with geochemical confirmation. Earth and Planetary Science Letters 206 (3–4), 529–540.

Ewing, T.E., Caran, C.S., 1982. Late Cretaceous volcanism in south and central Texas: stratigraphic, structural and seismic models. Gulf Coast Association of Geological Societies Transactions 32, 137–145.

Fialin, M., 1988. Modification of Philibert–Tixier ZAF correction for geological samples. X-ray Spectrometry 17 (3), 103–106.

Fisher, R.V., Schmincke, H.-U., 1984. Pyroclastic Rocks. Springer, Heidelberg, Germany. 472 pp.

Frank, T.D., Arthur, M.A., 1999. Tectonic forcings of Maastrichtian ocean–climate evolution. Paleoceanography 14 (2), 103–117.

Galloway, W.E., 1989. Genetic stratigraphic sequences in basin analysis: II. Application to Northwest Gulf of Mexico Cenozoic basin. AAPG Bulletin 73 (2), 143–154.

Gardin, S., 2002. Late Maastrichtian to early Danian calcareous nannofossils at Elles (northwest Tunisia): a tale of one million years across the K/T boundary. Palaeogeography, Palaeoclimatology, Palaeoecology 178 (3–4), 211–231.

Gardin, S., Monechi, S., 1998. Paleoecological change in middle to low latitude calcareous nannoplankton at the Cretaceous/Tertiary boundary. Bulletin de la Société Géologique de France 169 (5), 709–723.

Gartner, S., 1996. Calcareous nannofossils at the Cretaceous–Tertiary boundary. In: MacLeod, N., Keller, G. (Eds.), Cretaceous–Tertiary Boundary Mass Extinction: Biotic and Environmental Changes. Norton Press, New York, pp. 27–48.

Gingele, F.X., 1996. Holocene climatic optimum in southwest Africa—evidence from the clay mineral record. Palaeogeography, Palaeoclimatology, Palaeoecology 122 (1–2), 77–87.

Goto, K., Tada, R., Tajika, E., Bralower, T.J., Hasegawa, T., Matsui, T., 2004. Evidence for ocean water invasion into the Chicxulub crater at the Cretaceous/Tertiary boundary. Meteoritics and Planetary Science 39 (7), 1233–1247.

Grauby, O., Petit, S., Decarreau, A., Baronnet, A., 1993. The beidellite–saponite series: an experimental approach. European Journal of Mineralogy 5 (4), 623–635.

Güven, N., 1988. Smectites. In: Bailey, S.W. (Ed.), Hydrous Phyllosilicates (Exclusive of Micas), Reviews in Mineralogy, vol. 19. Mineralogical Society of America, pp. 347–403.

Håkansson, E., Thomsen, E., 1999. Benthic extinction and recovery patterns at the K/T boundary in shallow water carbonates, Denmark. Palaeogeography, Palaeoclimatology, Palaeoecology 154 (1–2), 67–85.

Hallam, A., Wignall, P.B., 1999. Mass extinctions and sea-level changes. Earth-Science Reviews 48 (3–4), 217–250.

Hansen, T.A., Farrand, R.B., Montgomery, H.A., Billman, H.G., Blechschmidt, G.L., 1987. Sedimentology and extinction patterns across the Cretaceous–Tertiary boundary interval in east Texas. Cretaceous Research 8 (3), 229–252.

Hansen, T.A., Farrell, B.R., Upshaw III, B., 1993a. The first 2 million years after the Cretaceous–Tertiary boundary in east Texas: rate and paleoecology of the molluscan recovery. Paleobiology 19 (2), 251–265.

Hansen, T.A., Upshaw III, B., Kauffman, E.G., Gose, W., 1993b. Patterns of molluscan extinction and recovery across the Cretaceous–Tertiary boundary in east Texas: report on new outcrops. Cretaceous Research 14 (6), 685–706.

Hargrove, D.C., Engelhardt, D.W., 1997. Palynology of the Maastrichtian/Danian boundary at Savannah River Site, South Carolina. Sedimentary Geology 108 (1–4), 121–140.

Hennebert, M., Dupuis, C., 2003. Use of cyclostratigraphy to build a high-resolution time-scale encompassing the Cretaceous–Palaeogene boundary in the Aïn Settara section (Kalaat Senan, central Tunisia). Geobios 36 (6), 707–718.

Henriksson, A.S., 1996. Calcareous nannoplankton productivity and succession across the Cretaceous–Tertiary boundary in the Pacific (DSDP Site 465) and Atlantic (DSDP Site 527) oceans. Cretaceous Research 17 (4), 451–477.

Herbert, T.D., 1999. Toward a composite orbital chronology for the Late Cretaceous and early Paleocene GPTS. Philosophical Transactions — Royal Society. Mathematical, Physical and Engineering Sciences 357 (1757), 1891–1905.

Herbert, T.D., Premoli-Silva, I., Erba, E., Fischer, A.G., 1995. Orbital chronology of Cretaceous–Paleocene marine sediments. In: Berggren, W.A., Kent, D.V., Aubry, M.-P., Hardenbol, J. (Eds.), Geochronology, Time Scales and Global Stratigraphic Correlation, Special Publication, vol. 54. Society of Economic Paleontologists and Mineralogists, Tulsa, Oklahoma, pp. 81–93.

Heymann, D., Yancey, T.E., Wolbach, W.S., Thiemens, M.H., Johnson, E.A., Roach, D., Moecker, S., 1998. Geochemical markers of the Cretaceous–Tertiary boundary event at Brazos River, Texas, USA. Geochimica et Cosmochimica Acta 62 (1), 173–181.

Hildebrand, A.R., Penfield, G.T., Kring, D.A., Pilkington, M., Camargo, A.Z., Jacobsen, S.B., Boynton, W.V., 1991. Chicxulub crater: a possible Cretaceous/Tertiary boundary impact crater on the Yucatán peninsula, Mexico. Geology 19 (9), 867–871.

Iverson, R.H., 1997. The physics of debris flows. Reviews of Geophysics 35 (3), 245–296.

Izett, G.A., 1990. The Cretaceous/Tertiary boundary interval, Ration basin, Colorado and New Mexico, and its content of shock-metamorphosed minerals: evidence relevant to the K/T boundary impact-extinction event. Special Paper, vol. 249. Geological Society of America, Boulder, Colorado. 100 pp.

Jarvis, I., Murphy, A.M., Gale, A.S., 2001. Geochemistry of pelagic and hemipelagic carbonates: criteria for identifying systems tracts and sea-level change. Journal of the Geological Society, London 158 (4), 685–696.

Jeans, C.V., Long, D., Hall, M.A., Bland, D.J., Cornford, C., 1991. The geochemistry of the Plenus Marls at Dover, England: evidence of fluctuating oceanographic conditions and of glacial control during the development of the Cenomanian–Turonian $d^{13}C$ anomaly. Geological Magazine 128 (6), 603–632.

Jiang, M.J., Gartner, S., 1986. Calcareous nannofossil succession across the Cretaceous/Tertiary boundary in east-central Texas. Micropaleontology 32 (3), 232–255.

Johnson, K.R., 2002. Megaflora of the Hell Creek and lower Fort Union Formations in the western Dakotas: Vegetational response to climate change, the Cretaceous–Tertiary boundary event, and rapid marine transgression. In: Hartman, J.H., Johnson, K.R., Nichols, D.J. (Eds.), The Hell Creek Formation and the Cretaceous–Tertiary Boundary in the Northern Great Plains—An Integrated Continental Record of the end of the Cretaceous, Special Paper, vol. 361. Geological Society of America, Boulder, Colorado, pp. 329–392.

Kamo, S.L., Krogh, T.E., 1995. Chicxulub crater source for shocked zircon crystals from the Cretaceous–Tertiary boundary layer, Saskatchewan: evidence from new U–Pb data. Geology 23 (3), 281–284.

Kastner, M., 2003. Oceanic minerals: their origin, nature of their environment, and significance. Proceedings of the National Academy of Science 96 (7), 3380–3387.

Keller, G., 1989a. Extended Cretaceous/Tertiary boundary extinctions and delayed population change in planktic foraminifera from Brazos River, Texas. Paleoceanography 4 (3), 287–332.

Keller, G., 1989b. Extended period of extinctions across the Cretaceous/Tertiary boundary in planktonic foraminifera of continental-shelf sections: implications for impact and volcanism theories. Geological Society of America Bulletin 101 (11), 1408–1419.

Keller, G., 1992. Paleoecologic response of Tethyan benthic foraminifera to the Cretaceous–Tertiary boundary transition. In: Takayanagi, Y., Saito, T. (Eds.), Studies in Benthic Foraminifera. Tokai University Press, Tokio, pp. 77–91.

Keller, G., Lindinger, M., 1989. Stable isotopes, TOC, and $CaCO_3$ record across the Cretaceous/Tertiary Boundary at El Kef, Tunisia. Palaeogeography, Palaeoclimatology, Palaeoecology 73 (3–4), 243–265.

Keller, G., Stinnesbeck, W., 1996. Sea-level changes, clastic deposits, and megatsunamis across the Cretaceous–Tertiary boundary. In: MacLeod, N., Keller, G. (Eds.), Cretaceous–Tertiary Boundary Mass Extinction: Biotic and Environmental Changes. Norton Press, New York, pp. 415–450.

Keller, G., Li, L., MacLeod, N., 1995. The Cretaceous/Tertiary boundary stratotype section at El Kef, Tunisia: how catastrophic was the mass extinction? Palaeogeography, Palaeoclimatology, Palaeoecology 119 (3–4), 221–254.

Keller, G., Li, L., Stinnesbeck, W., Vicenzi, E., 1998a. The K/T mass extinction, Chicxulub and the impact-kill effect. Bulletin de la Société Géologique de France 169 (4), 485–489.

Keller, G., Adatte, T., Stinnesbeck, W., Stüben, D., Kramar, U., Berner, Z., Li, L., von Salis Perch-Nielsen, K., 1998b. The Cretaceous–Tertiary transition on the shallow Saharan Platform of southern Tunisia. Geobios 30 (7), 951–975.

Keller, G., Adatte, T., Stinnesbeck, W., Rebolledo-Vieyra, M., Fucugauchi, J.U., Kramar, U., Stüben, D., 2004. Chicxulub impact predates the K–T boundary mass extinction. Proceedings of the National Academy of Science 97 (1), 1–6.

Kennedy, W.J., Landman, W.J., Christensen, C.W.A., Hancock, J.M., 1998. Marine connections in North America during the late Maastrichtian: paleogeographic significance of Jeletzkytes nebrascensis Zone cephalopod fauna from the Elk Butte Member of the Pierre Shale, SE Dakota and NE Nebraska. Cretaceous Research 19 (6), 745–775.

Kerr, M., Eyles, N., 1991. Storm-deposited sandstones (tempestites) and related ichnofossils of the Late Ordovician Georgian Bay Formation, southern Ontario, Canada. Canadian Journal of Earth Sciences 28 (2), 266–282.

Kettrup, B., Deutsch, A., 2003. Geochemical variability of the Yucatán basement: constraints from crystalline clasts in Chicxulub impactites. Meteoritics and Planetary Science 38 (7), 1079–1092.

Kettrup, B., Deutsch, A., Ostermann, M., Agrinier, P., 2000. Chicxulub impactites: geochemical clues to the precursor rocks. Meteoritics and Planetary Science 35 (6), 1229–1238.

Klaver, G.T., Van Kempen, T.M.G., Bianchi, F.R., 1987. Green spherules as indicators of the Cretaceous/Tertiary boundary in Deep Sea Drilling Project Hole 603B. Deep Sea Drilling Project. Initial Reports 93, 1039–1047.

Kletetschka, G., Wasilewski, P.J., Ocampo, A.C., Pope, K.O., 2001, Magnetic properties of the ejecta blanket from the Chicxulub impact crater: analog for robotic exploration of similar deposits on Mars (abstract). Spring Meeting, American Geophysical Union, #P32A-07.

Koeberl, C., MacLeod, K.G. (Eds.), 2002, Catastrophic Events and Mass Extinctions: Impacts and Beyond. Special Paper, 356, Geological Society of America, Boulder, Colorado. 746 pp.

Koeberl, C., Sigurdsson, H., 1992. Geochemistry of impact glasses from the K/T boundary in Haiti: relation to smectites and a new type of glass. Geochimica et Cosmochimica Acta 56, 2113–2129.

Kößler, P., Herrle, J.O., Appel, E., Erbacher, J., Hemleben, C., 2001. Magnetic records of climatic cycles from mid-Cretaceous hemipelagic sediments of the Vocontian Basin, SE France. Cretaceous Research 22 (4), 321–331.

Kramar, U., 1997. Advances in energy-dispersive X-ray fluorescence. Journal of Geochemical Exploration 58, 73–80.

Krogh, T.E., Kamo, S.L., Bohor, B.F., 1993a. Fingerprinting the K/T impact site and determining the time of impact by U–Pb dating of single shocked zircons from distal ejecta. Earth and Planetary Science Letters 119 (3), 425–429.

Krogh, T.E., Kamo, S.L., Sharpton, V.L., Marin, L.E., Hildebrand, A.R., 1993b. U–Pb ages of single shocked zircons linking distal K/T ejecta to the Chicxulub crater. Nature 366, 731–734.

Lawton, T.F., Shipley, K.W., Aschoff, J.L., Giles, K.A., Vega, F.J., 2005. Basinward transport of Chicxulub ejecta by tsunami-induced backflow, La Popa basin, northeastern Mexico, and its implications for distribution of impact-related deposits flanking the Gulf of Mexico. Geology 33 (2), 81–84.

Lehmann, T.M., 1990. Paleosols and the Cretaceous/Tertiary transition in the Big Bend region of Texas. Geology 18 (4), 362–364.

MacLeod, K.G., Huber, B.T., Pletsch, T., Röhl, U., Kucera, M., 2001. Maastrichtian foraminiferal and paleoceanographic changes on Milankovitch timescales. Paleoceanography 16 (2), 133–154.

MacQuaker, J.H.S., Gawthorpe, R.L., Taylor, K.G., Oates, M.J., 1998. Heterogeneity, stacking patterns and sequence stratigraphic interpretation in distal mudstone successions: examples from the Kimmeridge Clay Formation, UK. In: Schieber, J., Zimmerle, W., Sethi, P.S. (Eds.), Shales and Mudstones: I. Basin Studies, Sedimentology, and Paleontology. Schweizerbart, Stuttgart, Germany, pp. 163–186.

Maher, B.A., Thompson, R., Hounslow, M.W., 1999. Introduction. In: Maher, B.A., Thompson, R. (Eds.), Quaternary Climates, Environments and Magnetism. Cambridge University Press, Cambridge, United Kingdom, pp. 1–48.

Mai, H., Speijer, R.P., Schulte, P., 2003. Calcareous index nannofossils (coccoliths) of the earliest Paleocene originated in the late Maastrichtian. Micropaleontology 49 (2), 189–195.

Martínez-Ruiz, F., Ortega-Huertas, M., Palomo-Delgado, I., Acquafredda, P., 1997. Quench textures in altered spherules from the Cretaceous–Tertiary boundary layer at Agost and Caravaca, SE Spain. Sedimentary Geology 113 (1–2), 137–147.

Martínez-Ruiz, F., Ortega-Huertas, M., Kroon, D., Smit, J., Palomo-Delgado, I., Rocchia, R., 2001a. Geochemistry of the Cretaceous–Tertiary boundary at Blake Nose (ODP Leg 171B). In: Kroon, D., Norris, R.D., Klaus, A. (Eds.), Western North Atlantic Paleogene and Cretaceous Paleoceanography, Special Publication, vol. 183. Geological Society of London, London, United Kingdom, pp. 131–148.

Martínez-Ruiz, F., Ortega-Huertas, M., Palomo-Delgado, I., 2001b. Climate, tectonics and meteoritic impact expressed by clay mineral sedimentation across the Cretaceous–Tertiary boundary at Blake Nose, Northwestern Atlantic. Clay Minerals 36 (1), 49–60.

Martínez-Ruiz, F., Ortega-Huertas, M., Palomo-Delgado, I., Smit, J., 2001c. K–T boundary spherules from Blake Nose (ODP Leg 171B) as a record of the Chicxulub ejecta deposits. In: Kroon, D., Norris, R.D., Klaus, A. (Eds.), Western North Atlantic Paleogene and Cretaceous Paleoceanography, Special Publication, vol. 183. Geological Society of London, London, United Kingdom, pp. 149–161.

Martínez-Ruiz, F., Ortega-Huertas, M., Palomo-Delgado, I., Smit, J., 2002. Cretaceous–Tertiary boundary at Blake Nose (Ocean drilling Program Leg 171B): a record of the Chicxulub impact ejecta. In: Koeberl, C., MacLeod, K.G. (Eds.), Catastrophic Events and Mass Extinctions: Impacts and Beyond, Special Paper, vol. 356. Geological Society of America, Boulder, Colorado, pp. 189–200.

Martini, E., 1971. Standard Tertiary and Quarternary calcareous nannoplankton zonation. In: Farinacci, A. (Ed.), Second International Planktonic Conference Proceedings. Technoscienza, Rome, pp. 739–785.

Mayer, H., Appel, E., 1999. Milankovitch cyclicity and rock-magnetic signatures of palaeoclimatic change in the Early Cretaceous Biancone Formation of the Southern Alps, Italy. Cretaceous Research 20 (2), 189–214.

Montanari, A., 1991. Authigenesis of impact spheroids in the K/T boundary clay from Italy: new constraints for high-resolution stratigraphy of terminal Cretaceous events. Journal of Sedimentary Petrology 61 (3), 315–339.

Montanari, A., Koeberl, C., 2000. Impact Stratigraphy. Lecture Notes in Earth Sciences, vol. 93. Springer, Heidelberg, Germany. 364 pp.

Montgomery, H.A., Pessagno, E., Soegaard, K., Smith, C., Muñoz, I., Pessagno, J., 1992. Misconceptions concerning the Cretaceous/Tertiary boundary at the Brazos River, Falls County, Texas. Earth and Planetary Science Letters 109 (3–4), 593–600.

Moore, D.M., Reynolds, R.C., 1997. X-ray Diffraction and the Identification and Analysis of Clay Minerals. Oxford University Press, Oxford. 378 pp.

Mulder, T., Alexander, J., 2001. The physical character of subaqueous sedimentary density flows and their deposits. Sedimentology 48 (2), 269–299.

Müller, J., Oberhänsli, H., Melles, M., Schwab, M., Rachold, V., Hubberten, H.-W., 2001. Late Pliocene sedimentation in Lake Baikal: implications for climatic and tectonic change in SE Siberia. Palaeogeography, Palaeoclimatology, Palaeoecology 174 (4), 305–326.

Newman, A.C.D., Brown, A.C.D., 1987. The chemical constitution of clays. In: Newman, A.C.D. (Ed.), Chemistry of Clays and Clay Minerals, Mineralogical Society Monograph, vol. 6. Longman Scientific, London, United Kingdom, pp. 1–128.

Odin, G.S., 1992. New stratotypes for the Paleogene, the Cretaceous/Paleogene, Eocene/Oligocene and Paleogene/Neogene boundaries. Neues Jahrbuch für Geologie und Paläontologie, Abhandlungen 186 (1–2), 7–20.

Olsson, R.K., Liu, G., 1993. Controversies on the placement of the Cretaceous–Paleogene boundary and the K/T mass extinction of planktonic foraminifera. Palaios 8, 127–139.

Olsson, R.K., Liu, C., van Fossen, M., 1996. The Cretaceous–Tertiary catastrophic event at Millers Ferry, Alabama. In: Ryder, G., Fastovsky, D., Gartner, S. (Eds.), The Cretaceous–Tertiary Boundary Event and Other Catastrophes in Earth History, Special Paper, vol. 307. Geological Society of America, Boulder, Colorado, pp. 263–277.

Olsson, R.K., Wright, J.D., Miller, K.G., 2001. Paleobiogeography of *Pseudotextularia elegans* during the latest Maastrichtian global warming event. Journal of Foraminiferal Research 31 (3), 275–282.

Ortega-Huertas, M., Palomo-Delgado, I., Martínez-Ruiz, F., Gonzalez, I., 1998. Geological factors controlling clay mineral patterns across the Cretaceous–Tertiary boundary in Mediterranean and Atlantic sections. Clay Minerals 33 (3), 483–500.

Ortega-Huertas, M., Martínez-Ruiz, F., Palomo-Delgado, I., Chamley, H., 2002. Review of the mineralogy of the Cretaceous–Tertiary boundary clay: evidence supporting a major extraterrestrial catastrophic event. Clay Minerals 37 (3), 395–411.

Pardo, A., Ortiz, N., Keller, G., 1996. Latest Maastrichtian and Cretaceous–Tertiary foraminiferal turnover and environmental changes at Agost, Spain. In: MacLeod, N., Keller, G. (Eds.), Cretaceous–Tertiary Boundary Mass Extinction: Biotic and Environmental Changes. Norton Press, New York, pp. 139–171.

Perch-Nielsen, K., 1985. Mesozoic calcareous nannofossils. In: Saunders, J.B., Bolli, H.M., Perch-Nielsen, K. (Eds.), Plankton Stratigraphy. Cambridge University Press, Cambridge, United Kingdom, pp. 329–426.

Petschick, R., Kuhn, G., Gingele, F.X., 1996. Clay mineral distribution in surface sediments of the South Atlantic: sources, transport, and relation to oceanography. Marine Geology 130 (3), 203–229.

Pope, K.O., Ocampo, A.C., Fischer, A.G., Alvarez, W., Fouke, B.W., Webster, C.L., Vega, F.J., Smit, J., Fritsche, A.E., Claeys, P., 1999. Chicxulub impact ejecta from Albion Island, Belize. Earth and Planetary Science Letters 170 (4), 351–364.

Pospichal, J.J., 1996a. Calcareous nannoplankton mass extinction at the Cretaceous/Tertiary boundary: an update. In: Ryder, G., Fastovsky, D., Gartner, S. (Eds.), The Cretaceous–Tertiary Boundary Event and Other Catastrophes in Earth History, Special Paper, vol. 307. Geological Society of America, Boulder, Colorado, pp. 335–360.

Pospichal, J.J., 1996b. Calcareous nannofossils and clastic sediments at the K/T boundary, northeastern Mexico. Geology 24 (3), 255–258.

Remane, J., Keller, G., Hardenbol, J., Ben Haj Ali, M., 1999. Report on the international workshop on Cretaceous–Paleogene transitions. Episodes 22 (1), 47–48.

Ricken, W., 1994. Complex rhythmic sedimentation related to third-order sea-level variations: Upper Cretaceous, Western Interior Basin, USA. In: de Boer, P.L., Smith, D.G. (Eds.), Orbital Forcing and Cyclic Sequences, Special Publication, vol. 19. Blackwell, Oxford, International, pp. 167–193.

Robinson, S.G., 1993. Lithostratigraphic applications for magnetic susceptibility logging of deep-sea sediment cores: examples from ODP Leg 115. In: Hailwood, E.A., Kidd, R.B. (Eds.), High Resolution Stratigraphy, Special Publication, vol. 70. Geological Society of London, London, United Kingdom, pp. 65–98.

Ryder, G., Fastovsky, D., Gartner, S. (Eds.), 1996. The Cretaceous–Tertiary Event and Other Catastrophes in Earth history, Special Paper, vol. 307. Geological Society of America, Boulder, Colorado. 556 pp.

Salge, T., Tagle, R., Claeys, P., 2000, Accretionary lapilli from the K–T boundary site of Guayal, Mexico: preliminary insights of expansion plume formation (abstract). 63th Annual Meeting, Meteoritical Society, #5124 (CD-ROM).

Scheffers, A., Kelletat, D., 2003. Sedimentologic and geomorphologic tsunami imprints worldwide—a review. Earth-Science Reviews 63 (1–2), 83–92.

Schieber, J., 1998. Sedimentary features indicating erosion, condensation, and hiatuses in the Chattanooga Shale of central Tennessee: relevance for sedimentary and stratigraphic evolution. In: Schieber, J., Zimmerle, W., Sethi, P.S. (Eds.), Shales and Mudstones: I. Basin Studies, Sedimentology, and Paleontology. Schweizerbart, Stuttgart, Germany, pp. 187–215.

Schmitz, B., 1992. Chalcophile elements and Ir in continental Cretaceous–Tertiary boundary clays from the Western Interior of the USA. Geochimica et Cosmochimica Acta 56, 1695–1703.

Schulte, P., 2003, The Cretaceous–Paleogene transition and Chicxulub impact ejecta in the northwestern Gulf of Mexico: paleoenvironments, sequence stratigraphic setting, and target lithologies [online at: www.ubka.uni-karlsruhe.de/cgi-bin/psview?document=2003/bau-geo/10]. PhD Thesis, University of Karlsruhe, Karlsruhe, Germany. 204 pp.

Schulte, P., Kontny, A., 2005. Chicxulub ejecta at the Cretaceous–Paleogene (K–P) boundary in Northeastern México. In: Hörz, F., Kenkmann, T., Deutsch, A. (Eds.), Large Meteorite Impacts: III. Special Paper, vol. 384. Geological Society of America, Boulder, Colorado, pp. 191–221.

Schulte, P., Stinnesbeck, W., Stüben, D., Kramar, U., Berner, Z., Keller, G., Adatte, T., 2003. Fe-rich and K-rich mafic spherules from slumped and channelized Chicxulub ejecta deposits at the northern La Sierrita area, NE Mexico. International Journal of Earth Sciences 92 (1), 114–142.

Schuraytz, B.C., Sharpton, V.L., Marín, L.E., 1994. Petrology of impact-melt rocks at the Chicxulub multiring basin, Yucatán, Mexico. Geology 22 (10), 868–872.

Schutter, S.R., 1998. Characteristics of shale deposition in relation to stratigraphic sequence systems tracts. In: Schieber, J., Zimmerle, W., Sethi, P.S. (Eds.), Shales and Mudstones: I. Basin Studies, Sedimentology, and Paleontology. Schweizerbart, Stuttgart, Germany, pp. 79–108.

Schwarzacher, W., 2000. Repetitions and cycles in stratigraphy. Earth-Science Reviews 50 (3–4), 51–75.

Self-Trail, J.M., 2001. Biostratigraphic subdivision and correlation of upper Maastrichtian sediments from the Atlantic Coastal Plain and Blake Nose, western Atlantic. In: Kroon, D., Norris, R.D., Klaus, A. (Eds.), Western North Atlantic Paleogene and Cretaceous Paleoceanography, Special Publication, vol. 183. Geological Society of London, London, United Kingdom, pp. 93–110.

Shanmugam, G., 1997. The Bouma sequence and the turbidite mind set. Earth-Science Reviews 42 (4), 201–229.

Shau, Y.H., Feather, M.E., Essene, E.J., Peacor, D.R., 1991. Genesis and solvus relations of submicroscopically intergrown paragonite and phengite in a blueschist from Northern California. Contributions to Mineralogy and Petrology 106 (3), 367–378.

Shiki, T., Kumon, F., Inouchi, Y., Kontani, Y., Sakamoto, T., Tateishi, M., Matsubara, H., Fukuyama, K., 2000. Sedimentary features of the seismo-turbidites, Lake Biwa, Japan. Sedimentary Geology 135 (1–4), 37–50.

Sigurdsson, H., Leckie, R.M., Acton, G.D., 1997. Caribbean volcanism, Cretaceous/Tertiary impact, and ocean climate history: synthesis of Leg 165. Proceedings of the Ocean Drilling Program. Initial Reports 165, 377–400.

Smit, J., 1999. The global stratigraphy of the Cretaceous–Tertiary boundary impact ejecta. Annual Reviews in Earth and Planetary Sciences 27, 75–113.

Smit, J., Alvarez, W., Montanari, A., Claeys, P., Grajales-Nishimura, J.M., 1996. Coarse-grained, clastic sandstone complex at the K/T boundary around the Gulf of Mexico: deposition by tsunami waves induced by the Chicxulub impact? In: Ryder, G., Fastovsky, D., Gartner, S. (Eds.), The Cretaceous–Tertiary Boundary Event and Other Catastrophes in Earth History, Special Paper vol. 307. Geological Society of America, Boulder, Colorado, pp. 151–182.

Smit, J., Gaast, S.V.D., Lustenhouwer, W., 2004. Is the transition impact to post-impact rock complete? Some remarks based on XRF scanning, electron microprobe, and thin section analyses of the Yaxcopoil-1 core in the Chicxulub crater. Meteoritics and Planetary Science 39 (7), 1113–1126.

Smith, C.C., Pessagno, E.A., 1973. Planktonic Foraminifera and Stratigraphy of the Corsicana Formation (Maestrichtian), North-central Texas. Special Publication, vol. 12. Cushman Foundation for Foraminiferal Research, Ithaca, New York. 68 pp.

Speijer, R.P., Van der Zwaan, G.J., 1996. Extinction and survivorship of southern Tethyan benthic foraminifera across the Cretaceous/Paleogene boundary. In: Hart, M.B. (Ed.), Biotic Recovery from Mass Extinction Events, Special Publication, vol. 102. Geological Society of London, London, United Kingdom, pp. 343–371.

Stinnesbeck, W., Keller, G., Adatte, T., López-Oliva, J.-G., MacLeod, N., 1996. Cretaceous–Tertiary boundary clastic deposits in NE Mexico: bolide impact or sea-level lowstand? In: MacLeod, N., Keller, G. (Eds.), The Cretaceous–Tertiary Boundary Mass Extinction: Biotic and Environmental Events. Norton Press, New York, pp. 471–517.

Stüben, D., Kramar, U., Berner, Z., Stinnesbeck, W., Keller, G., Adatte, T., 2002a. Trace elements, stable isotopes, and clay mineralogy of the Elles II K/T boundary section in Tunisia: indications for sea level fluctuations and primary productivity. Palaeogeography, Palaeoclimatology, Palaeoecology 178 (3–4), 321–345.

Stüben, D., Kramar, U., Berner, Z., Eckhardt, J.-D., Stinnesbeck, W., Keller, G., Adatte, T., Heide, K., 2002b. Two PGE anomalies above the Cretaceous/Tertiary boundary at Beloc/Haiti: geochemical context and consequences for the impact scenario. In: Koeberl, C., MacLeod, K.G. (Eds.), Catastrophic Events and Mass Extinctions: Impacts and Beyond, Special Paper, vol. 356. Geological Society of America, Boulder, Colorado, pp. 163–188.

Sweet, A.R., Braman, D.R., 2001. Cretaceous–Tertiary palynofloral perturbations and extinctions within the Aquilapollenites Phytogeographic Province. Canadian Journal of Earth Sciences 38 (2), 249–269.

Thiry, M., 2000. Palaeoclimate interpretation of clay minerals in marine deposits: an outlook from the continental origin. Earth-Science Reviews 49 (1), 201–221.

Van Wagoner, J.C., Mitchum, R.M., Campion, K.M., Rahmanian, V.D., 1990. Siliciclastic sequence stratigraphy in well logs, cores, and outcrops: concepts for high-resolution correlation of time and facies. Methods in Exploration, vol. 7. American Association of Petroleum Geologists, Tulsa, Oklahoma. 53 pp.

Wdowiak, T.J., Armendarez, L.P., Agresti, D.G., Wade, M.L., Wdowiak, Y.S., Claeys, P., Izett, G.A., 2001. Presence of an iron-rich nanophase material in the upper layer of the Cretaceous–Tertiary boundary clay. Meteoritics and Planetary Science 36 (1), 123–133.

Wignall, P.B., 2001. Large igneous provinces and mass extinctions. Earth-Science Reviews 53 (1–2), 1–33.

Worm, H.U., Banerjee, S.K., 1987. Rock magnetic signature of the Cretaceous–Tertiary boundary. Geophysical Research Letters 14 (11), 1083–1086.

Wray, D.S., Gale, A.S., 1993. Geochemical correlation of marl bands in Turonian chalks of the Anglo-Paris Basin. In: Hailwood, E.A., Kidd, R.B. (Eds.), High-Resolution Stratigraphy, Special Publication, vol. 70. Geological Society of London, London, United Kingdom, pp. 211–226.

Yancey, T.E., 1996. Stratigraphy and depositional environments of the Cretaceous/Tertiary boundary complex and basal section, Brazos River, Texas. Gulf Coast Association of Geological Societies Transactions 46, 433–442.

Yancey, T.E., 2002. Carbonate ejecta spherules in Cretaceous–Tertiary boundary deposits, Brazos River, Texas (abstract). Annual Meeting, Geological Society of America, #178-112.

Yuretich, R., Melles, M., Sarata, B., Grobe, H., 1999. Clay minerals in the sediments of the Lake Baikal: a useful climate proxy. Journal of Sedimentary Research 69 (3), 588–596.

Zachos, J.C., Arthur, M.A., Dean, W.E., 1989. Geochemical and paleoenvironmental variations across the Cretaceous/Tertiary boundary at Braggs, Alabama. Palaeogeography, Palaeoclimatology, Palaeoecology 69, 245–266.